PONTIFICIA UNIVERSIDAD CATOLICA DE CHILE

ESCUELA DE INGENIERIA

3D MODELING OF SITE-CITY EFFECTS USING SPECTRAL ELEMENT METHOD. APPLICATION TO VIÑA DEL MAR CITY, CHILE

VALERIA PAZ SOTO MONCADA

Thesis submitted to the Office of Research and Graduate Studies in partial fulfillment of the requirements for the Degree of Master of Science in Engineering

Advisor:

ESTEBAN SÁEZ ROBERT

Santiago de Chile, (December, 2019)

PONTIFICIA UNIVERSIDAD CATOLICA DE CHILE

ESCUELA DE INGENIERIA

3D MODELING OF SITE-CITY EFFECTS USING SPECTRAL ELEMENT METHOD. APPLICATION TO VIÑA DEL MAR CITY, CHILE

VALERIA PAZ SOTO MONCADA

Members of the Committee:

ESTEBAN SÁEZ ROBERT

ROSITA JÜNEMANN URETA

CAROLINA MAGNA VERDUGO

CÉSAR SÁEZ NAVARRETE

Thesis submitted to the Office of Research and Graduate Studies in partial fulfillment of the requirements for the Degree of Master of Science in Engineering

Santiago de Chile, (December, 2019)

“La realidad está ahí y nosotros en ella, entendiéndola a nuestra manera, pero en ella”

ACKNOWLEDGMENTS

This work was supported by the FONDEF project D10E1027 and CIGIDEN (Research Center for Integrated Disaster Risk Management) FONDAP 15110017.

First, I would like to thank my supervisor, Professor Esteban Sáez, for always be willing to guide me and enlightening me during this thesis. I'll be forever thankful for all the given opportunities throughout my masters.

I thank my friends Felipe, Laura, Danilo and Luis, for all the arduous work and great time that we had together during the long field days for the project. To Hugo and Pablo, thank you for the unconditional motivation and for being always my biggest supporters.

I'm very grateful for all the protection, guidance and love from my family during all my study years. Finally, I would like to dedicate this work to my grandfathers, especially to my late grandfather Mario, for their love and wisdom.

GENERAL INDEX

Page

LIST OF TABLES

Page

LIST OF FIGURES

Page

ABSTRACT

In recent years, seismic wave propagation analyses have become a powerful tool to evaluate the site effects in a given region. While many approaches are available, the Spectral Element Method (SEM) has been widely used for that purpose because of its flexibility and computational efficiency. Basin shape, material nonlinearity and heterogeneity are important effects; however, the multiple inter-actions between the soil and structures, known as site-city effects (SCI), can also play a crucial role in analyses of densely populated areas. There are many options to model this kind of interaction, especially if the buildings are partially embedded in the soil. This paper evaluates the importance of the proper SCI modeling against more standard uncoupled approaches, focusing on the local interaction between the soil and a group of buildings including inelastic soil behavior. We focus our work on the case of downtown Viña del Mar, a touristic coastal city of central Chile, where the observation of a reiterated distribution of damage in reinforced concrete buildings during two major earthquakes has motivated numerous studies. For that purpose, a realistic 3D numerical model of the area was created, considering the existing buildings. The open-source code SPEED was used to perform the wave propagation simulation, which combines the spectral element method with a discontinuous Galerkin approach. A geophysical study was conducted to estimate the model parameters; in addition, shear modulus degradation and damping curves were extracted from laboratory tests to account for the non-linearity of the soil. In general, the results indicate that the inclusion of the SCI is beneficial to the structure's response in most cases, and that the SCI modeling needs to consider the level of embedment to obtain more precise results.

Keywords: soil-city interaction effects, spectral element method, site effects

RESUMEN

En los últimos años, los análisis de propagación de ondas sísmicas se han convertido en una herramienta poderosa para evaluar los efectos del sitio en una región determinada. Entre varios enfoques, el Método del elementos espectrales (SEM, por sus siglas en inglés) se ha utilizado ampliamente con ese propósito, gracias a su flexibilidad y eficiencia computacional. Además de los efectos por forma de la cuenca, la no linealidad y heterogeneidad de los materiales, las múltiples interacciones entre el suelo y las estructuras, denominadas efectos sitio-ciudad (SCI), pueden desempeñar un papel crucial en áreas densamente pobladas. Sin embargo, hay muchas opciones para modelar este tipo de interacción, especialmente si los edificios están parcialmente enterrados en el suelo. Este artículo evalúa la importancia un adecuado modelado de los SCI frente a enfoques desacoplados más estándar, centrándose en la interacción local entre el suelo y un grupo de construcciones en una parte de una ciudad, incluido el comportamiento inelástico del suelo. En particular, enfocamos nuestro trabajo en el caso del centro de Viña del Mar, una ciudad turística costera de Chile central, donde la observación de una distribución de daños reiterada en edificios de hormigón armado durante dos grandes terremotos ha motivado numerosos estudios. Para ese propósito, se crea un modelo numérico 3D realista del área bajo estudio, considerando los edificios existentes. El programa de código abierto SPEED se utilizó para realizar la simulación de propagación de ondas, que combina el método SEM con el enfoque de Galerkin Discontinuo. Un estudio geofísico fue esencial para estimar los parámetros del modelo. Además, curvas de degradación del módulo de corte y amortiguamiento se extrajeron de pruebas de laboratorio, para tener en cuenta la no linealidad del suelo. En general, los resultados indican que la inclusión del SCI es beneficiosa para la respuesta de la estructura en la mayoría de los casos, y que el modelado necesita considerar el nivel de empotramiento para obtener resultados más precisos.

Palabras Clave: Efectos de interacción suelo-ciudad, método de los elementos espectrales, efectos de sitio

1 INTRODUCTION

The history of large earthquakes in Chile, were megathrust events are originated by the subduction process between the Nazca and the South-American plates, comes from ancestral times. In Central Chile, with 200 to 600 years of recurrence, the last tsunamigenic huge earthquake was in 1730. Three types of earthquakes are frequent in this area: interplate on the plate interface, intraplate intermediate depth, and shallow events. The depths of these earthquakes are variable and range from 15 to 55 kilometers. Near Valparaíso, two recent interplate earthquakes, M_w 8.2 in 1906 and M_w 8.0 1985, stroked the area (Ruiz & Madariaga, 2018).

After the observed damages in reinforced concrete buildings produced by the M_w 8.8 2010 Maule event, the last megathrust earthquake in South-Central Chile, the seismic normative in Chile for residential buildings at the time, NCh433, was updated with the supreme decree DS N°61 (Ministerio de Vivienda y Urbanismo, 2011). The supreme decree N° 61 added the Vs30 parameter (average shear wave velocity in the first 30 meters) to the seismic classification of subsoil.

Specifically, in the city of Viña del Mar, recurrent building damage has been observed during the last earthquakes that affected the area. Viña del Mar is a city located in the Valparaíso Region, in Central Chile. The downtown is above sediments composed mainly of sand with approximately 20 to 100 meters depths to the bedrock (Podestá, Sáez, Yáñez, & Leyton, 2019). This scenario facilitates the generation of site- effects, given the high impedance contrast between the soil and the bedrock.

The seismic damages at the city have been widely evaluated and described from structural analysis approaches, and the propensity of site effects, resulting from the geological setting that exists in the area, has generated numerous studies of microzonation as well (Aranda, Vidal, Alguacil, Navarro, & Valverde-Palacios, 2014; Carrasco & Nuñez, 2013; Jünemann, de la Llera, Hube, Cifuentes, & Kausel, 2015; Riddell, Wood, & de la Llera, 1987; Toledo, 2017). It was observed recurrent damage primarily affecting a sector of the basin, in the area associated with the Marga-Marga Fault and only affecting specific types of buildings.

This study has as main motivation to generate an evaluation of the seismic demand of buildings from a joint analysis of the whole problem, that is, of a system that takes into account the interaction between buildings and soil. In the case of densely populated cities, as downtown Viña del Mar, the interference of buildings in the wave propagation, denominated site-city interaction (SCI), can modify the ground motion and the structural response.

To fulfill this purpose, a regional seismic wave propagation study of the area was formulated. Among several empirical (based on previous observations) and physics-based methods to predict a ground motion, the numerical models emerge as an alternative to provide a realistic understanding of the phenomena (Smerzini, 2010). In this case, the simulation used the spectral elements method (SEM) combined with a domain discretization approach to model effectively the geometrical complexities of the problem.

To have a reliable local seismic response, it is necessary to determine the numerical parameters through a correct characterization of the materials in the problem (Smerzini, 2010). In particular, this study conducted an extensive geophysical campaign to characterize both soil and building parameters.

This study starts with the idea of generating a complete model of the city of Viña del Mar. Unfortunately, for computational resources, the domain had to be bounded to a reduced area, keeping representativeness of the overall problem. Then, this works focuses on locally assessing the SCI on the seismic demand of buildings. It is important to note that the study does not intend to deliver an accurate structural response of the buildings, due to the simplicity of the buildings, but instead to evaluate and compare their response by including the complex interaction effects.

Chapter 1 describes the motivation and objectives of this study. For a better understanding of the problem, the main concepts are described in the methodology. Section 2 contains a copy of the article “Numerical modeling of 3D site-city effects including partially embedded buildings using spectral element methods. Application to the case of Viña del Mar city, Chile”, submitted to Engineering Structures journal.

1.1 HYPOTHESIS

This main hypothesis is that site-city effects in densely urban scenarios play a significant role in the dynamic motion of the soil surface and structures. These effects could explain the localized damage of buildings in the central area of Viña del Mar, which is not fully explained with more simplistic approaches, and therefore they should not be neglected in the analysis.

1.2 OBJECTIVES

- General objective

The main goal of this study is to evaluate and quantify the contribution of the site-city interaction effects in the dynamic ground response and to compare the soil-structure interaction in the building's response in the city of Viña del Mar.

- Specific objectives
    - Create a realistic coupled 3D spectral element model of Viña del Mar city, which includes the soil, the basin, and existing buildings.
    - Estimate a simplified model for the structures. Determine their geometry and their dynamic properties. Analysis of geophysical data obtained with surface waves techniques and satellite imagery.
    - Evaluate the ground motion by the wave propagation of selected Ricker wavelets. Peak ground acceleration (PGA) and Velocity (PGV), Arias intensity.
    - Compare the structural response of the fully coupled model with the response of fixed-base models, in terms of node drift, maximum roof displacement, etc.

1.3 LITERATURE REVIEW: SITE-CITY INTERACTION

As defined by (Taborda, 2010), the site-city interaction (SCI) effects in a group of buildings involve both the modification of the ground motion and the alteration of the structural response of each building, due to multiple interactions that occur as the structures are inserted in the soil media. In comparison with a fixed base analysis, two main effects are involved in this soil-structure system: the inertial interaction effects, that affect the dissipation of energy through radiation damping and hysteretic soil damping; and the kinematic effects, that cause uncoupled motion between the foundation and the adjacent soil (NEHRP, 2012).

Inertial interaction refers to the effects of inertial forces produced by seismic accelerations in the structure, where the base shear, bending moment, and torsions increase, generating relative displacements between the free-field and the foundation. This reaction can create flexibility and energy dissipation by hysteretic behavior or radiation. On the other hand, kinematic interaction occurs when the motion at the foundation, which is more rigid than the ground, deviates from the free-field motions. In the case of buildings where their foundations are under the ground, there is also an embedment effect, where the movement that reaches the base is different from what would be found in the free-field.

First studies related to SCI focused on the role urban environment had on the duration and amplitude of the ground motion (e.g., Chávez-García & Cárdenas-Soto, 2002; Wirgin & Bard, 1996), as they realized that the study of the response of a site was always disconnected from the response of the buildings. The first studies were based on the change that the inclusion of buildings, as objects, could have on the propagation of surface waves and thus affect both the intensity and duration of the ground-motion.

For that reason, they used mainly idealized cities to understand the problem and its controlling parameters. In 2006, (Kham, Semblat, Bard, & Dangla, 2006) conducted a parametric study on the density of buildings and their natural frequencies with simplified 2D models.

More recent studies that incorporated the basin shape effects revealed the importance of the double resonance (Sahar, Narayan, & Kumar, 2015). However, studies that include the SCI effects in the assessment of structural responses are limited and recent, which indicates that it is a complex phenomenon, but that its importance is being taken into account in the Earthquake Engineering community. Two different studies considered the SCI to create an uncoupled model for the evaluation of the nonlinear time history analysis in buildings (Lu, Tian, Wang, & Huang, 2018) and to estimate the role of the 3D basin shape effects in the structural response (Kumar & Narayan, 2019). While they found a general reduction of the seismic responses, the first found that a few buildings will suffer more damage with the inclusion of SCI effects.

Finally, while the level of embedment is included in the analysis of soil-structure interaction and its effect generates, in general, a reduction in base motions (Amini & Shadlou, 2011; Avilés & Pérez-Rocha, 1998; NEHRP Consultants Joint Venture, 2012), when modeling the SCI effects, the depth of burial has been ignored. This study also aims to evaluate the influence of this parameter.

1.4 METHODOLOGY

To fulfill the objectives of the study, a realistic 3D spectral element model was created. To obtain reliable results, it was necessary to have a proper definition of the properties of its main three components: the basin, the bedrock and existing buildings within the study area. Hence, the methodology is divided into three parts: First, a detailed explanation of the formulation used in the code to obtain the results, SPEED: the spectral element method, and its implementation of the Discontinuous Galerkin approach. Second, the description of the procedure followed to obtain the properties for the soil, focusing on the geophysical survey that was part of the FONDEF D10E1027 project. Third, a description of the obtained seismic behavior of buildings and how we estimated the governing parameters.

1.4.1 SPEED

The SPEED program is an open-source code that combines the spectral element method (SEM) with a non-conforming discretization of the domain to solve seismic wave propagation problems numerically. The SEM method is a high variational method, using high-order interpolants, based on the weak formulation of the Elastodynamics equations that work on the time domain (Smerzini, 2010).

1.4.1.1 Governing equations in Elastodynamics

For a 3D space, $\Omega \subset \mathbb{R}^3$, with Lipschitz boundary, $\Gamma = \partial\Omega$. The boundary $\Gamma = \Gamma_D \cup \Gamma_N \cup \Gamma_{NR}$, is composed by Γ_D, where the displacement vector u is prescribed or Dirichlet conditions are applied, Γ_N where the external forces p or Neumann conditions are applied and Γ_{NR}, where non-reflecting boundary conditions are imposed. Based on the principle of virtual work, the equilibrium equation used in SPEED is stated as follow:

$\rho \frac{\partial^2 u}{\partial t^2} + 2\rho\xi \frac{\partial u}{\partial t} + \rho\xi^2 u - \nabla \cdot \sigma(\mathrm{u}) = \mathrm{f} \text{ in } \Omega \times (0, T]$ (1-1)

This equation differs from the original elastodynamic equation since it adds $2\rho\xi \frac{\partial u}{\partial t}$ and $\rho\xi^2 u$, two equivalent volume forces that recreate the spatially varying visco-elastic materials, characterized by a decay factor ξ. With this modification, all the frequencies components are approximately equally attenuated, according to the Q factor:

$Q = Q_0 \frac{f}{f_0} = \pi \frac{f_0}{\xi} \frac{f}{f_0} = \frac{1}{2\xi}$ (1-2)

Besides, the boundary conditions for the problem are:

$u = 0$ on Γ_D, $\sigma(u)n = p^*$ on $\Gamma_N \cup \Gamma_{NR}$ (1-3)

Where n is the unit outward normal vector to Γ and

$p^* = \begin{cases} p & on\ \Gamma_N \\ \rho(V_P - V_S)\left(\frac{\partial u}{\partial t} \cdot n\right) n + \rho V_S \frac{\partial u}{\partial t} & on\ \Gamma_{NR} \end{cases}$ (1-4)

That represents the absorbing boundary in Γ_{NR}. Additionally, the displacement $u = u_0$ and velocity $\frac{\partial u}{\partial t} = u_1$ are prescribed.

The spectral element method uses the weak formulation of the equilibrium equation. Then, multiplying the equation (1.1) for a regular function v, and integrating by parts over the domain Ω, the variational formulation reads as follow: $\forall t \in (0, T]$ find $u = u(t) \in V$ such that

$\frac{\partial^2}{\partial t^2}(\rho u, v) + A(u, v)_\Omega = (f, v)_\Omega + (p, v)_{\Gamma_N}$(1-5)

Where A is a bilinear form for the constitutive equation between stresses, σ and displacements, ε, defined as

$A(u, v)_\Omega = \big(\sigma(u), \varepsilon(v)\big)_\Omega$(1-6)

1.4.1.2 The Discontinuous Galerkin discretization

The Discontinuous Galerkin formulation is a non-conforming discretization technique that allows having both geometrical and polynomial flexibility on the domain. Is a time-independent spatial decomposition of the domain Ω in three levels, shown in Figure 1-1 (Antonietti, Mazzieri, Quarteroni, & Rapetti, 2012):

1. First level: The domain Ω is partitioned in k non-overlapping regions that can be geometrically non-conforming, i.e., the interface of two neighboring subdomains, $\gamma = \partial\Omega_{\mathrm{k}} \cap \partial\Omega_{\mathrm{l}}$, may not be a complete face of Ω_{k} or Ω_{l}.
2. Second level: Each subdomain, Ω_k, is partitioned on hexahedral elements for the 3D case, geometrically conforming.
3. Third level: On each mesh element, the Legendre-Gauss-Lobato (LGL) points that work as interpolation points for the high order polynomials and also as quadrature points for the numerical integration.

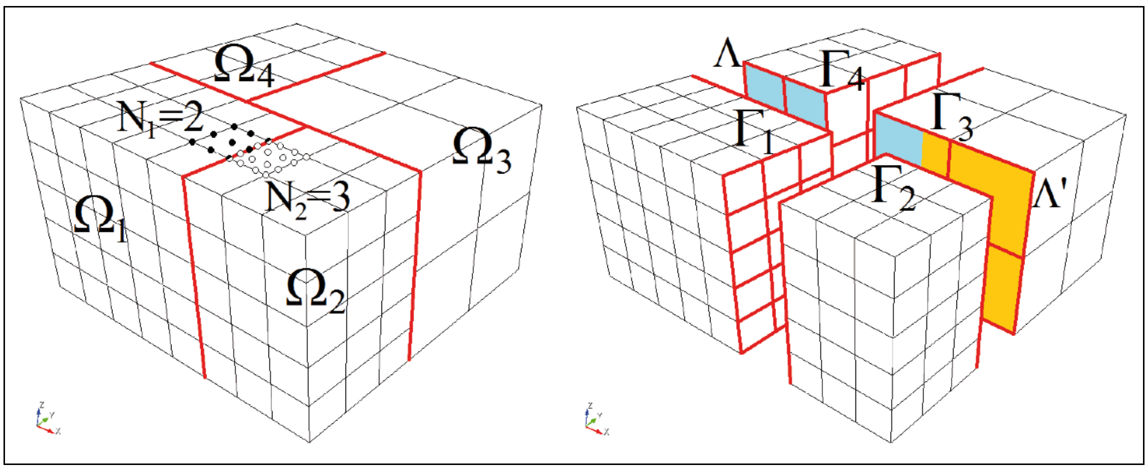

Figure 1-1: Non-conforming domain decomposition used in SPEED. Description of the three levels partitions (left) and the non-conforming interfaces (right). Obtained from (Mazzieri, Stupazzini, Guidotti, & Smerzini, 2013)

With that discretization, the variational formulation (Equation 1-5) is rewritten at the intersection of two neighboring elements belonging to different subdomains. The elastodynamic problem is then solved on each subdomain with transmission conditions of displacement and tractions across the interface (Antonietti, 2012).

In the developed model (Chapter 2.3) we take full advantage of this feature available on SPEED to use different element sizes through the model domain. Far from the surface and at bedrock level, the material is stiffer, deformation of elements is small, and the behavior is approximately elastic. Consequently, coarser elements could be used. Close to the surface, inelastic behavior is more pronounced because of lower confinement, and a finer mesh is required. Transitions between coarser a finer meshes were optimized to reduce the computational cost of the overall model thanks to this discontinuous Galerkin approach.

1.4.1.3 Plane incidence of waves

In our case, the seismic source, i.e., the subduction zone, is located at depths between 10-50 [kms]. For that reason, it is reasonable that the propagation wave may be simplified as a vertical incident plane wave, acting at the bottom of the model. Next, we described the implementation of this type of wave in SPEED. The displacement field, $u(z,t)$, generated by a distribution of body forces

$f(z,t) = \phi(t)\delta(z - z_0)e_i$ (1-7)

applied at the and acting on the plane $z = z_0$, is calculated as

$u_i(z,t) = \frac{1}{2\rho c} H\left(t - \frac{|z-z_0|}{c}\right) \int_0^{t-\frac{|z-z_0|}{c}} \phi(\tau) d\tau$ (1-8)

Where c is the propagation velocity, ρ the material density, and $H(\cdot)$ is the Heaviside function. The input is then $\phi(t)$, the prescribed incident velocity field:

$\phi(t) = 2\rho c \frac{\partial \bar{u}_i(t)}{\partial t}$ (1-9).

In the developed model, this vertical plane wave was introduced at about 200 [m] below the surface.

1.4.2 Site properties

This study was part of the Fondef+Andes 2.0 (FONDEF D10E1027) project, an applied research project titled “Technological Transfer to Sernageomin by the case study of San Antonio-Los Vilos seismotectonic segment”, a multidisciplinary work of civil engineers, geoscientists and investigators from the Pontificia Universidad Católica de Chile, Universidad de Concepción and SERNAGEOMIN (National Service of Geology and Mining). The results produced were Seismic Hazard maps of coastal cities of central Chile to contribute to the prevention of potential risks associated with seismic activity. The SIGAS or “Georeferenced Information System of Seismic Hazard” was implemented, a free-access website (http://sigas.sernageomin.cl). In particular, the next paragraphs describe the methodology followed to locally characterize soil conditions, necessary to the assessment of seismic hazard. In particular, the information generated for the Viña downtown area was directly used for the developed model.

To characterize the site effects, an extensive geophysical prospection was conducted. The purpose of the measurements was to determine the shear wave velocity profile at each site and its predominant period. In total, 232 measurements were analyzed at sites, limited by the city Los Vilos, IV region in the north, and by the town of Santo Domingo, V Region in the southern part. Among them, Viña del Mar, the focus of this study, was also measured.

The data was recorded with two types of digital seismometers: a set of 24 vertical geophones (4.5 Hz natural frequency) and a set of 10 vertical geophones (1.0 Hz natural frequency). Besides, to obtain the HVSR, two independent triaxial seismometers (0.3 Hz natural frequency) were used. The following sections will detail the methods used.

1.4.2.1 Surface Wave Techniques

The shear wave velocity profile (Vs) is critical to characterize the soil amplification at a determined site. The preferred techniques to obtain this profile are non-invasive methods based on the dispersion of surface waves, mainly because they are time and cost-effective in comparison to borehole methods, sharing similar results (Garofalo et al., 2016). The propagation of surface waves is governed by geometric dispersion: different wavelengths investigate different depths, hence, at each frequency, the phase velocity depends on the properties of the investigated part of the subsurface (Garofalo et al., 2016). The phase velocity dependency on the frequency or wavelength is called the dispersion curve.

In this case, we used combined source controlled (active, high frequencies) with ambient noise (passive, low frequencies) techniques, in 1D (linear) and 2D arrays. The linear arrays collected both ambient noise and active-noise tests, using a hammer for the seismic source. The 2D arrays were used only for passive noise recording.

The approaches used in this project are the frequency-wave number analysis or F-K (Kvaerna & Ringdahl, 1986) for both passive and active tests, the ESPAC analysis for linear passive tests (Hayashi, 2008) and the Spatial autocorrelation analysis (SPAC) for passive trials (Aki, 1957).

- Spectral Analysis F-K: This method assumes that a combination of ambient noise and plane waves, determined by his frequency (F) and wave number (K), cross the arrangement of receivers. The method can be benefited from both passive (useful in urban areas) and active sources. The response of the array is the combination of the receptor's signals, calculated by retarding the signals at each receiver to obtain the same arrival time, in terms of the array geometry. Then, it is possible to get the dispersion curve by calculating the energy spectra in the frequency-wave number domain.

- SPAC: The spatial autocorrelation method was developed by (Aki, 1957). This method is based on the spatial correlation of microtremors recorded at two stations. The spatial correlation coefficient varies as a Bessel function dependent on the frequency, phase velocity and receiver separation.
- ESPAC: (Hayashi, 2008). This method is derived from SPAC for linear arrays. Allows defining the dispersion curve for each frequency and phase velocity.

Figure 1-2(1) shows an example of a combined dispersion curve for a site in the city of Papudo. Obtained this dispersion curve, an inverse problem is generated to obtain the shear wave velocity profile, with the software Geopsy®. This inverse problem is based on the neighborhood algorithm (Wathelet, 2008), that search profiles that minimize the "misfit", or adjustment ratio, between the theoretical and observed dispersion curves. Figure 1-2(2) and (3) shows a range of adjusted dispersion curves and the best shear wave velocity profile up to 30 meters, respectively.

1.4.2.2 HVSR

The Nakamura method (Nakamura, 1989), or horizontal to vertical spectral ratio, relates the horizontal with vertical Fourier spectra of surface microtremor to obtain the predominant frequency of the soil, F_0 or is inverse, the predominant period, T_0.

It is assumed that the horizontal and vertical tremors, mainly composed by Rayleigh waves, a type of surface waves, are similar to each other and are amplified when they propagate through soft layers of soil. The transfer function, S_T, calculates this amplification, defined as:

$$S_T = \frac{S_{HS}}{S_{HB}} \quad (1\text{-}10)$$

S_{HS} is the horizontal microtremor spectrum on the surface and S_{HB} is the horizontal microtremor spectrum of the incident wave on the soil layers. Note that S_T, S_{HS}, S_{HB} are functions of the frequency. The same ratio can be defined with the vertical components:

$$E_S = \frac{E_{VS}}{E_{VB}} \quad (1\text{-}11)$$

To neglect the effect of the Rayleigh wave on the surface, Nakamura defines a modified transfer function, S_{TT}, by combining equations (1-10) and (1-11), and from observations assumes that the propagation on the basement is even in all directions, so $S_{HB} = E_{VB}$. Then, the transfer function can be estimated only with the surface microtremors, as:

$$S_{TT} = \frac{S_T}{E_S} = \frac{S_{HS}}{E_{VS}} \quad (1\text{-}12)$$

The peak in this transfer function corresponds to the predominant frequency of the site. In this study, the total record is divided into 60-seconds windows and the Stockwell transform is calculated for each window (Leyton, Ramírez & Vásquez, 2012). Then, the horizontal components are combined and the ratio between the horizontal and vertical spectra is calculated. The results are shown in Figure 1-2(5). It should also be noted that the peak amplitude also adds information on the impedance contrast that would exist between the sediment and the basement. The higher the peak amplitude, the greater the impedance contrast between the soil and basement materials (Leyton et al., 2013).

1.4.2.3 Site classification

The seismic classification of a site is established in Chile by the Supreme Decree D.S. No. 61. The parameter Vs30, the harmonic average shear-wave velocity in the first 30 meters from the surface, allows to estimate the stiffness of the soil at low deformations:

$$V_{s30} = \frac{\sum_{i=1}^{n} h_i}{\sum_{i=1}^{n} \frac{h_i}{V_{s-i}}} \quad (1\text{-}13)$$

With this value, the soil is classified into five categories. However, this study used a modified classification, where the Vs30 is replaced by the amount of $V_{s<900}$, defined as the average speed including soils with Vs less than 900 m/s before reaching a depth of 30m. Once the values of Vs30 (or $V_{s<900}$) and the predominant periods T0 (or its reciprocal the predominant frequency F0) are obtained for each point, each site is seismically classified according to the criteria indicated in Table 1-1. To apply this classification, first entrance is by the column of Vs30. If the T0 criteria is met, the classification is as indicated. If this last criterion is not satisfied, the classification degrades one level to the next row of the table.

Table 1-1: Proposed seismic classification.

Soil type	**Vs30 (m/s)**	**T_0 (s)**
A	>900	Flat or <0.15
B	500-900	Flat or <0.30
C	350-500	Flat or <0.40
D	180-350	<0.75
E	<180	/

The results were synthesized in a summary sheet for each site, described in Figure 1-2.

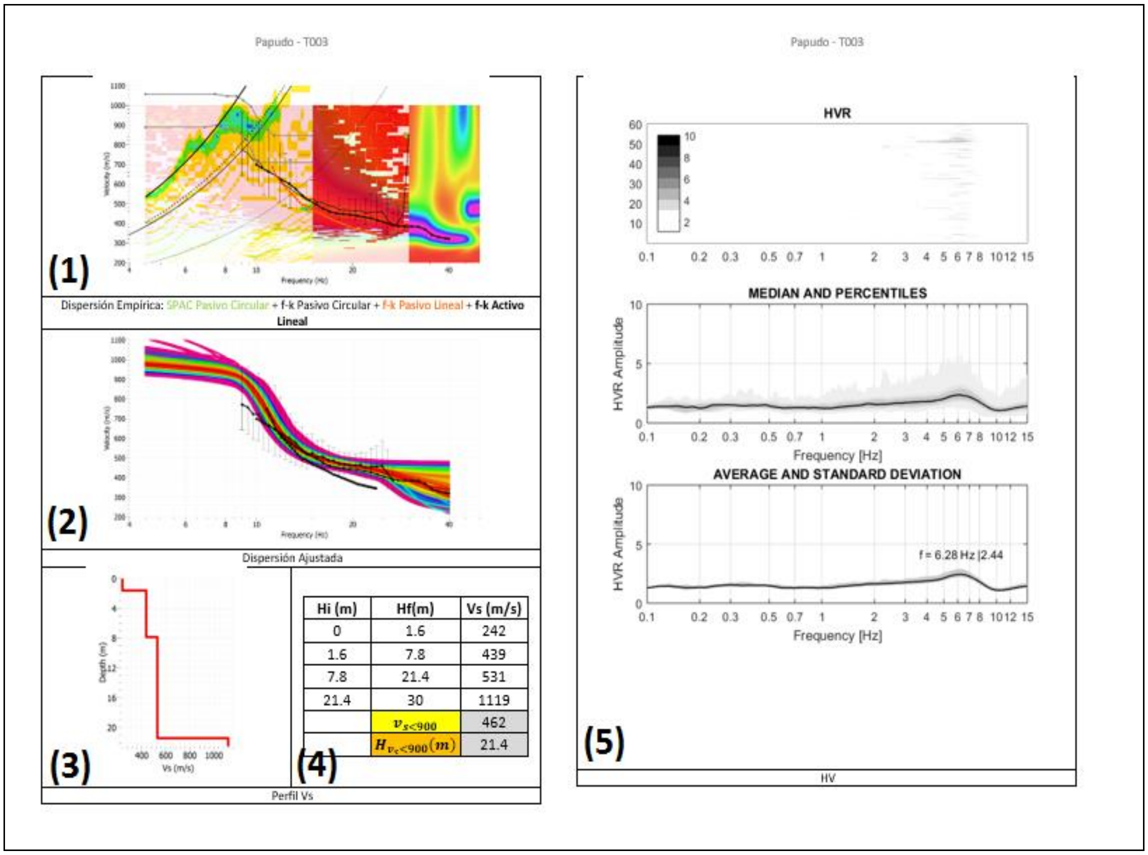

Figure 1-2: File generated for seismic classification of sites. (1) Observed and (2) Adjusted dispersion curves, (3) and (4) shear wave velocity profile, and (5) HVR for the obtention of the predominant period.

For the city of Viña del Mar, the discrete results for each site are summarized in Figure 1-3 (V_{s30}) and Figure 1-4 (F0). Besides, the analysis of these results allowed the formulation of a microzonation map for the city, represented in the figures with the same colors as the seismic classification.

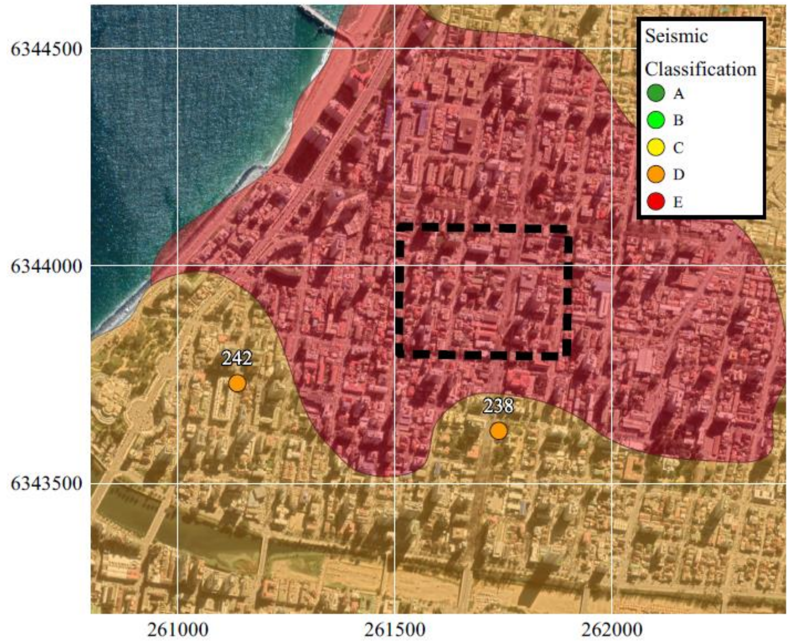

Figure 1-3: V_{s30} and seismic classification for sites in downtown Viña del Mar. Background colors represent the microzonation proposed as a result of the FONDEF project. The modeled area enclosed in black (WGS84 - UTM 19S).

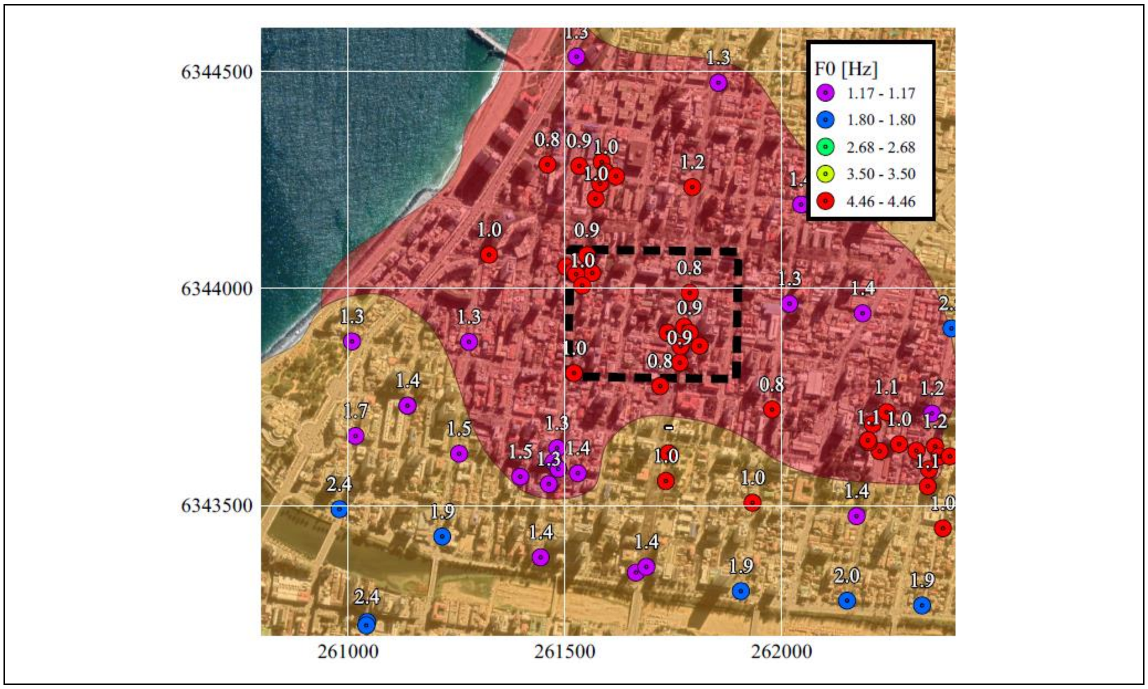

Figure 1-4: F0 for sites in downtown Viña del Mar. Results obtained by (Podestá et al., 2019), used for the model, are also mapped. Background colors represent the microzonation proposed as a result of the FONDEF project. The modeled area enclosed in black (WGS84 - UTM 19S).

1.4.2.4 Non-linearity

The previous characterization allowed describing each layer of soil based on its stiffness, which can be obtained from the following relationship:

$$G_{max} = \rho V_s^2 \quad (1\text{-}14)$$

Where ρ is the density of the soil and V_s is the small-strains shear-wave velocity. When the ground is excited by seismic loads, shear stresses and deformations are large enough to induce non-linear behavior of the soil. Then, another relevant parameter to characterize the material in a seismic motion analysis corresponds to the level of damping (D), associated with the energy dissipated. Assuming that the seismic load is idealized as a loop of load cycle, Figure 1-5a shows the hysteretic stress-strain relationship and the definition of the secant stiffness, G, and the calculation of hysteretic damping, D. Then, the stiffness degradation and damping curves relate to the material degradation and energy dissipation achieved for each strain value (Figure 1-5b). These curves are determined mainly with laboratory tests.

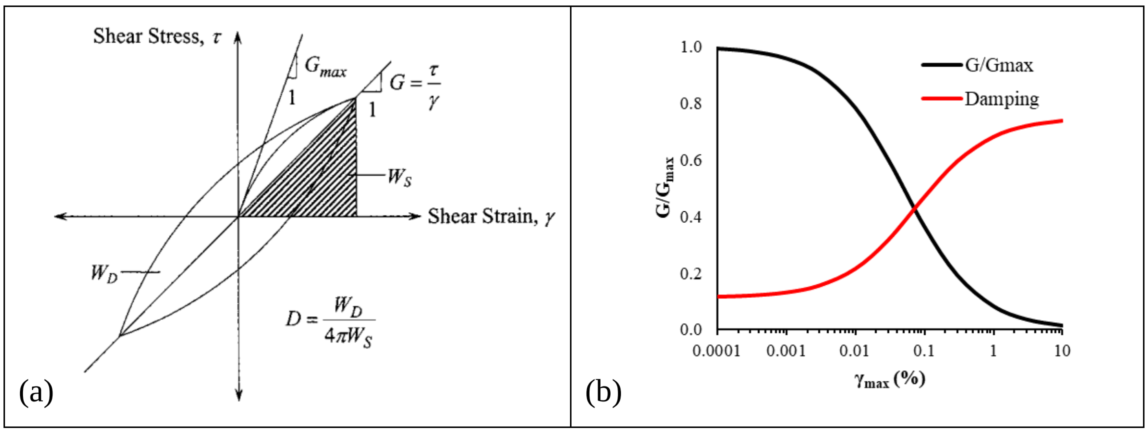

Figure 1-5: (a) hysteretic loop for one cycle of a dynamic load. Obtained from (Zhang, Andrus, & Juang, 2005) (b) Idealized modulus degradation and damping curves.

In our study, these curves were determined for 100 and 200 kPa confinements by cyclic triaxial and resonant column tests. However, one of the main factors affecting the creation of these curves corresponds to the effective confinement, σ'_m, depending on the vertical σ'_v and horizontal stresses σ'_h (Zhang et al., 2005):

$$\sigma'_m = \frac{(\sigma'_v + 2\sigma'_h)}{3} \quad (1\text{-}15)$$

Our soil domain had a wide range of confinements, from the surface up to more than 100 meters depth, and it was also necessary to add the confinement increment due to the inclusion of buildings superficially. Then, the methodology suggested by (Zhang et al.,

2005) was used to find a hyperbolic model for the G/G_{max} relationship that allows adding the influence of confinement. Proposed expression is described in Section 2.3.2.

1.4.3 Building properties

Due to a large number of buildings in the city of Viña del Mar that this study intended to model, the estimation of parameters must be as simple as possible. Therefore, its geometry and spatial distribution were estimated based on free satellite imagery. To characterize the seismic behavior of a building, the fundamental vibration frequency (or period) is essential. The methodology for obtaining and validating this parameter, is described below.

In Chile, the estimation of fundamental frequencies of a building is, in general, correlated with geometrical parameters: height, number of stories, or floor-plan dimensions. In our study, we chose the relation between the fundamental period and the number of stories (without considering underground levels) due to its simplicity and good agreement with prior data (Jünemann et al., 2015).

Table 1-2: N/T relation from different authors for the city of Viña del Mar.

Author, Year	N/T relation
Midorikawa, 1990	0.049
Riddell et al., 1987	0.050
Aranda et al., 2014	0.045
Jünemann et al., 2015	0.050

This relationship has been studied by various investigations in the past. Table 1-2 shows the main results for four authors (Aranda et al., 2014; Jünemann et al., 2015; Midorikawa, 1990; Riddell et al., 1987). They are very similar. As firs attempt, we decided to use the following relation to estimate the fundamental period of the soil T in terms of the number of stories, N:

$$T\ [\mathrm{s}] = \frac{\mathrm{N}}{20} \quad (1\text{-}16)$$

For the validation of this relationship in specific, we conducted a geophysical study using ambient vibrations, similar to the one used to obtain the predominant periods in soils. This simplified method assumes that ambient noise is the input to the building structure, and will be amplified, at different frequencies, depending on the dynamic response of the building itself (Panzera, Lombardo, & Muzzetta, 2013). The ambient motion does not need a vibration source and can contain several vibration modes (Midorikawa, 1990).

A field campaign was conducted in the city of Viña del Mar in December 2018. In total, 79 buildings were measured. Figure 1-6 shows the location of the buildings measured, distributed in the southwest area of the Viña del Mar plan, which also coincides with the more densely constructed area.

We used a seismometer Tromino 3G®, which has a natural frequency of 0.3 Hz, to measure the accelerations in three perpendicular directions. Ambient vibrations were collected for 30 minutes with a sampling frequency of 128 Hz. The instrument was aligned perpendicular to the sides of the building, centered and supported directly on the surface of the top floor.

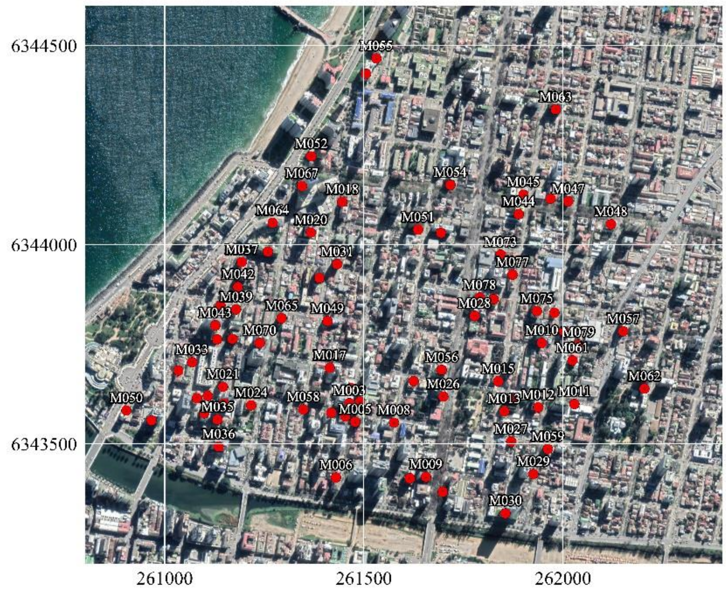

Figure 1-6: Distribution of geophysical characterization of building for the obtention of fundamental frequency in Viña del Mar (WGS84 - UTM 19S).

To find the resonance frequency, the data was divided into 60-second windows, and, for each component (north, east and vertical), the fast Fourier transform was calculated. The amplification is generated mainly on the horizontal components of the motion of the highest floor (Panzera et al., 2013). The North and East components represent the two preferential directions of the sides of the building. Then, the resonant frequency is estimated, in its first mode, as the lowest frequency between the two horizontal components (the most flexible).

At each building, information about the number of stories and underground levels, type and year of construction was collected. Most of these buildings are shear-wall of reinforced concrete buildings.

As an example, Figure 1-7 shows the result for an 8-story and one underground level building. In colors, the average above the windows used for each component. According to Equation 1-16, the estimated period should be 0.40 s. The observed period from the geophysical characterization is about 0.43 s. The aggregated results are shown in Chapter 2.

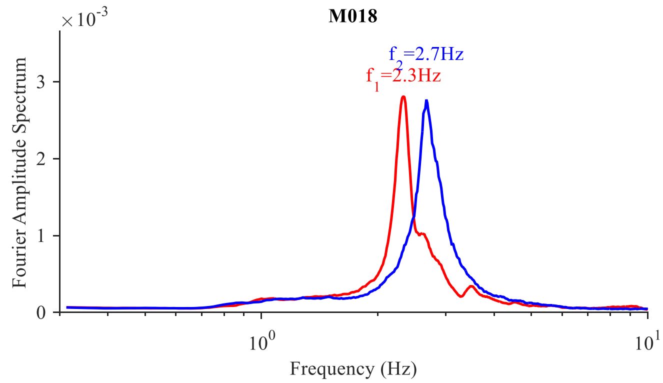

Figure 1-7: Fourier Amplitude Spectrum for a selected building. Each trace (red and blue) represent one of the horizontal components, associated with the main directions of the building. The fundamental frequency then corresponds to the lowest value (the most flexible).

1.5 RESULTS AND FUTURE WORK

This work aims to understand the local effects produced by the multiple interactions between embedded buildings and the surrounding soil in a realistic urban setting, the city of Viña del Mar. For this purpose, three different models were created: a fully coupled 3D model, a 3D model without the buildings, and 1D columns to separate the effects. Also, the response of structures is evaluated in terms of the level of embedment.

The current Chilean seismic design code D.S. N° 61 (Ministerio de Vivienda y Urbanismo, 2011b)) does not explicitly limit the damage in buildings. However, the seismic deformations are restricted in terms of the maximum roof displacement and maximum displacement between floors. Therefore, these parameters were used to compare the structural response in the three different models.

The SCI effects are, in general, beneficial for most buildings. However, a few will suffer more damage, similar behavior found by (Lu et al., 2018; Taborda, 2010). From the findings of the study, the following is clear: in larger buildings the response would be indifferent to the level of embedding of the base and, in these cases, the inclusion of site-city effects is beneficial. On the other hand, in buildings of less than 12 stories the total embedment of the base generates a significant decrease in the response. Thus, it is important to take into account the underground levels.

While the evaluation of SCI effects on buildings is complex, it is believed that the increase in confinement stresses resulting from the difference between the excavated soil and the weight of the building would be key to explain the decrease in response. With the increase in confinement, the properties of the soil under the foundation are stiffer, thus reducing deformation. This also highlights the need to consider the nonlinearity of the soil.

On the other hand, regarding soil to site resonance, the foundation flexibility modeled by the coupled approach introduces a frequency shift from resonance for buildings ID195 and ID450, avoiding this kind of amplification. From our results we believe that underground levels have a significant influence on the building's response, future research will focus on a more detailed quantification of this specific aspect of the SCI problem.

Group effects, on the other hand, have to do with the interaction between buildings. Although the buildings themselves generate an obvious interference in their surroundings, their influence on other buildings was not clear. Future work pretends to expand the domain to more dense and large areas to introduce basin boundaries and therefore include surface wave generation and their effects on SCI.

In conclusion, the objective of this study was partially fulfilled due to computational and time resources. The ability to assess the large-scale effects of the basin and group effects will be explored in future stages of the research. However, since this model was based on a realistic scenario, it would be useful for the evaluation of buildings more prone to sustain damage.

SCI effects are, in general, beneficial, so including them in the seismic design would be cost-effective. However, they correspond to complex effects that require a large amount of information from both the site and buildings to obtain reliable behavior. This study aimed to provide a way to evaluate these effects through simple estimates and to evaluate some parameters that govern the problem, putting a special emphasis on the role of the non-lineal soil behavior in the problem.

The results found prove that the SCI effects, the multiple interference of the group of buildings in the wave propagation, could influence the structural response of each other. Therefore, the seismic design might consider in the future the spatial distribution of other building in its surroundings, as well the SCI explicitly in their dynamic analysis. Consequently, the assessment of group effects on the seismic design of new buildings might be included in the Urban Planning of densely populated cities like Viña del Mar.

Moreover, the FONDEF D10E1027 project, which partially funds this research, generated a large amount of freely available information about local site conditions, in major populated areas of coastal central Chile. This information enclosed a much broader segment than just the city of Viña del Mar, but with the same considerations, this work could be replicated to make 3D models in smaller towns, in which buildings proliferate in recent years.

2 NUMERICAL MODELING OF 3D SITE-CITY EFFECTS INCLUDING PARTIALLY EMBEDDED BUILDINGS USING SPECTRAL ELEMENT METHODS. APPLICATION TO THE CASE OF VIÑA DEL MAR CITY, CHILE

2.1 INTRODUCTION

The city of Viña del Mar, located in the central coastal area of Chile, is one of the most densely populated cities of the country. Its downtown is built in a sedimentary valley where saturated fluvial medium sands predominate. This stratigraphy promotes site effects, given the significant impedance contrast between sandy soils and bedrock. The earthquake-induced damage observed in buildings in the city during the last three major events and documented by previous investigations are of great interest because they are reiterated, located in a narrow area, and affected medium-height buildings. While several authors have studied the site effects in the area (e.g. Toledo, 2017), most focus on the one-dimensional problem of amplification controlled by the sediment thickness; however, the localized damage suggest that the amplification should be explained by a more complex phenomenon.

Prior studies in other cities have illustrated the importance of 3D site effects. For instance, three-dimensional studies in alluvial basins that have a small spatial extension and a closed-shape in the Gubbio plain, Italy, showed that they were remarkable differences on the amplification between 3D and 2D approaches, explained by the relevance of the generation and propagation of surface waves due to the basin shape (Smerzini, Paolucci, & Stupazzini, 2011). A 3D model that includes the basement shape in Viña del Mar developed by Podestá, et al. (2019) considered this concept. However, the tridimensional seismic amplification found was of second-order, and the concentration of damage shown in the buildings suggested a site-structure resonance problem (coupling of the natural frequency of the buildings with the predominant frequency of the soil column underneath them).

Apart from the basin shape or material heterogeneity, the interference of the buildings in the wave propagation may play a significant role in the case of densely populated cities. These effects, denominated site-city interaction (SCI), reduce or amplify the seismic motion. As defined by Taborda (2010), the site-city interaction effects in a group of buildings involve both the modification of the ground motion and the alteration of the structural response of each building, due to multiple interactions that occur as the structures are inserted in the soil media. In comparison with a fixed base analysis, two main effects are involved in this soil-structure system: the inertial interaction effects, that affect the dissipation of energy through radiation damping and hysteretic soil damping; and the kinematic effects, that cause uncoupled motion of the foundation and the adjacent soil (NEHRP, 2012).

First studies related to SCI focused on the role the urban environment had on the duration and amplitude of the ground motion (e.g. Chávez-García & Cárdenas-Soto, 2002; Wirgin & Bard, 1996), by means of understanding the problem and its controlling parameters with idealized cities. Kham, Semblat, Bard, & Dangla (2006) conducted a parametric study on the density of buildings and their natural frequencies with simplified 2D models. More recent studies that incorporated the basin shape effects revealed the importance of the resonance between the 3D basin and 3D structures of the city (Sahar, Narayan, & Kumar, 2015). However, studies that include the SCI effects in the assessment of structural responses are limited and recent, which indicates that it is a complex phenomenon, although its importance is being considered in the Earthquake Engineering community. Two different investigations included the SCI to create an uncoupled model for the evaluation of the nonlinear time history analysis in buildings (Lu, Tian, Wang, & Huang, 2018) and to estimate the role of the 3D basin shape effects in the structural response (Kumar & Narayan, 2019). While they found a general reduction of the seismic responses, the first found that a few buildings will suffer more damage with the inclusion of SCI effects.

The objectives of this study aim to evaluate and quantify the contribution of the site-city interaction in the dynamic ground response and to compare the different approaches to model the soil-structure interaction for the building structures. A realistic 3D model of a selected area in the segment was created with the open-source code software, based on the spectral element method. The spectral element method is a powerful tool that combines the modeling of complex geometries with an exponential convergence of the solution. For available computational resources and runtime limitations, a region of about 400x300m^2 was selected, representing typical urban density across the city in terms of the number and height of buildings. This area includes some of the most damaged buildings identified in the last two earthquakes that affected the city. The fully coupled model consists of the soil, the basin bedrock, and existing buildings.

To obtain soil properties and to characterize the basin, a geophysical survey was conducted, based on surface wave techniques and gravimetry. Inelastic soil behavior is included in the model with the Linear Equivalent approach. Two types of laboratory tests were performed to describe the nonlinear cyclic behavior of the soil. To describe the local configuration and to estimate the elastic properties of the buildings in the area, information based on high-resolution satellite imagery and obtained from Google Earth® were combined. Additionally, an ambient vibration analysis was applied to several buildings to develop a simple relation between the dynamic properties and its geometry.

A comparison between the structural response of the buildings computed from the 3D coupled model and from fixed-based uncoupled models is used to assess the role of the structures' local interaction with the soil at various levels of embedment. The results are expected to help to determine if the site-city effects could be neglected or, on the contrary, could contribute to the increase of the structural demands based on the results of the case study of Viña del Mar.

2.2 AVAILABLE INFORMATION AND MICROVIBRATION SURVEY

The city of Viña del Mar is a coastal city located in the central part of Chile. It is the fourth largest city of the country, with a population of 334,248 inhabitants, increasing up to 432,258 during the summer months (December to February) (INE, 2017). The total surface of the city is 49.15 km^2, while the downtown area, best known as "Plan of Viña del Mar", has a surface of 5.04 km^2.

The regional geology of the area is formed by an intrusive basement with an overlying of semi-consolidated marine terraces, both outcropping in the outermost part of the segment. On top of these sequences, there is 30 to 110 meters of thickness of unconsolidated fluvial sediments composed of sand, silt, and gravel. These sediments are produced by the Marga Marga river, which flows into the Pacific Ocean in the south part of the city (Grimme & Álvarez, 1964).

2.2.1 Geotechnical characterization of the Viña del Mar Basin

A detailed geophysical survey was conducted in the area by Podestá et al. (2019). Shear wave velocity profiles were obtained at several sites, combining source controlled (active) techniques with ambient noise (passive) techniques. Based on the geophysical and geological characterization, we decided to create a simplified model defined by two geotechnical units: the basin bedrock and the overlying soil. The Equation 2-1 was proposed to characterize the shear wave velocity profile for the sediments in the area as a function of the depth. Using the unit weight of the soil and an assumption of the at-rest lateral earth coefficient, the equation could be transformed into a function of the effective vertical stress, with σ_v' in kPa (Equation 2-2).

$v_s(z)$=158.62 $z^{0.2}$ (2-1)

$v_s(\sigma_v)$=88.97$\sigma_v'^{0.2}$ (2-2)

Additionally, the Nakamura method (Nakamura, 1989) also known as the horizontal-to-vertical spectral ratio was used to estimate the predominant frequency in distributed points within the studied area. The interpolated results are shown in Fig. 1a, in terms of the predominant period T0 (in seconds). To obtain the basin thickness, the measured principal frequencies were used to extend a homogeneous soil column using the Eq. (1) to fit the first elastic soil period to the measured value. The location of the basin is a combination of this basement depth with a Digital Elevation Model (DEM) of 5 meters as spatial resolution shown in Figure 2-1b. The elevation varies from a few meters above the sea level in downtown Viña del Mar, where this investigation is focused, to 70 meters above the sea level in the northern part of the segment. The thickness of the soil layer controls the depth of the basin in the central area because the elevation is almost constant in this part of the city.

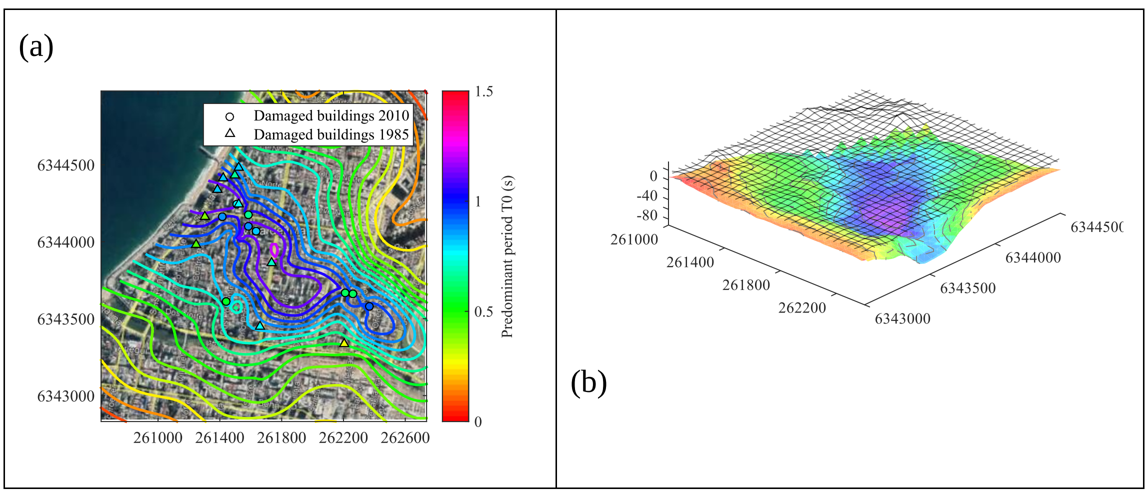

Figure 2-1 (a) Contours of predominant periods T0 (s) obtained by interpolation of several HVSR and significantly damaged buildings during previous earthquakes according to Riddell et al. (1990) and Jünemann (2015); (b) bedrock and topography of the Viña del Mar central area.

2.2.2 Building Inventory

The last two major earthquakes that struck the area occurred in 1985 and 2010. Regarding the M_w 8.0, 1985 earthquake, Riddell et al. (1990) conducted an inventory of 145 reinforced concrete buildings that had five or more stories in the city at the time. The buildings, constructed from 1950 to 1984, had five to ten stories, and the structural configurations were predominantly shear walls. For tall buildings, mat foundations and continuous footing for lower-rise structures were preferred, usually founded 4 to 5 meters below the ground surface. The location of damaged buildings in the area is shown in Fig. 1a with a triangle shaped marker. Moderate to severely damaged buildings were located in the deepest part of the basin, and a significant portion of these buildings had 12 to 15 stories; damage was not observed in the high-rise buildings in the same area. This fact suggests that the damage may be related to the filter effect of soil around its predominant frequency compared to the fundamental frequency of the buildings. A more recent study, conducted by Jünemann et al., (2015), focused on damaged buildings with more than nine stories when the 2010, Mw 8.8 Maule Earthquake, struck in the south-central part of Chile. The damage affected primarily the lower floors from medium-high buildings, similar to the results observed during the 1985 earthquake. A statistical analysis showed that the foundation soil type was one of the most significant variables to correlate with the level of damage.

Today, the urban area of the city is characterized by approximately 680 buildings of 4 or more stories. Figure 2-2a shows the spatial distribution of buildings. Each building is included as a homogeneous block to simplify the model generation. Hence, the geometry and main dynamic properties (natural frequency of vibration) need to be estimated to develop realistic structure models. The number of stories and floor-plan dimensions were obtained with Google Earth® and the Google Street View® tool. The total height was determined by assuming a 2.5 meters inter-story height. This value has been checked against the DEM when available. The number of underground levels was adjusted case to case when possible, using as default two levels or 5 meters below the surface.

Both authors used the number of stories divided by 20 ($\lambda = 20$) to estimate the fundamental period of the structures. This equation allows a simple yet realistic approximation of Chilean reinforced concrete residential buildings, avoiding the development of a detailed structural model for a substantial collection of buildings. Ambient vibrations were recorded in 78 buildings in the city (see Figure 2-2) to validate this relation for Viña del Mar. The tests were performed using four seismometers Tromino®, positioned at the center of the top floor, oriented in the main two directions of the structure. The trace of 30 minutes was divided into windows of 60 seconds and analyzed in the range of 0.3 Hz to 10 Hz. The observation of the peaks in the Fourier Amplitude Spectra of the horizontal components of the velocity allows obtaining an estimator of the fundamental period of the structure.

Linear regressions were fitted to obtain the values that best describe the relationship between the number of stories of the buildings and their natural periods. A λ value of 18.0 was obtained by comparing the period with the number of stories, while $\lambda = 20$ improves the agreement if the basement levels are considered (red curve). This value agrees with the one found by Midorikawa (1990) in ambient vibration tests for buildings in Viña del Mar and Santiago. Of course, this expression is only an estimator of the building's vibrating period during the earthquake, which includes the contribution of non-structural walls and neglects any stiffness degradation due to the inelastic behavior of both structure and soil. However, it could be considered a lower bound of the longest seismic vibrating period. Both prior studies focused on a detailed structural analysis of the damaged buildings, but no particular attention was put on site-structure dynamical relations explaining damage concentration. In this paper, we explore the mutual influence of both the site and the soil on the observed damage.

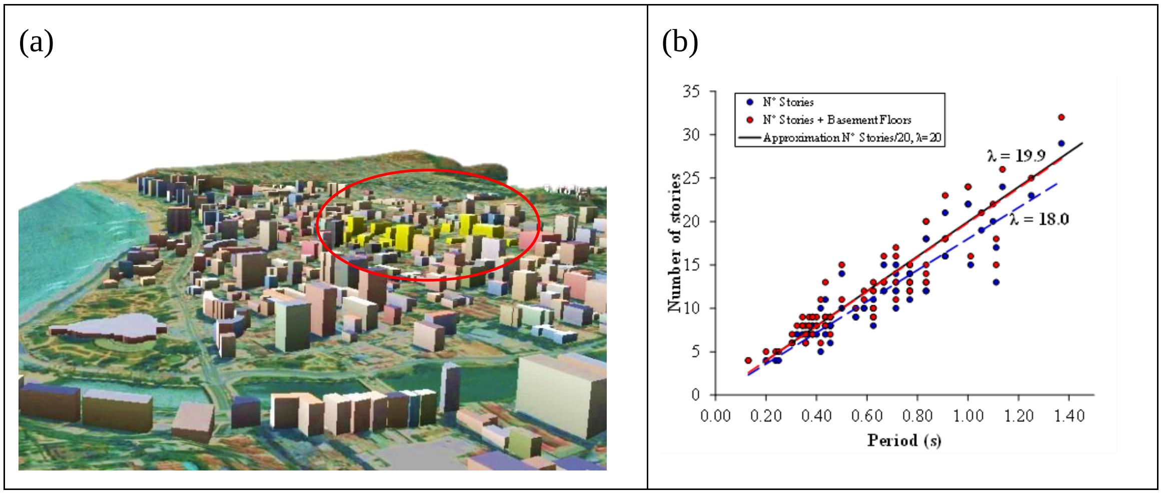

Figure 2-2: (a) Distribution of buildings in downtown Viña del Mar. The modeled buildings are shown in yellow. (b) Relation used for the prediction of the natural frequency of the buildings in terms of the number of stories.

2.3 MODEL

2.3.1 Spectral Element Method and Discontinuous Galerkin approach

The numerical simulation was performed using the SPEED program, a free code that uses the spectral element method (SEM) to solve the weak formulation of the Elastodynamics equations for elastic wave propagation problems (Mazzieri et al, 2013). The SEM is a generalization of the finite element model (FEM). Both discretize the space in hexahedral elements, but the SEM uses high order orthogonal polynomials as shape functions (Lagrange polynomials), contrary to the low order polynomials used in the FEM, thus increasing the numerical accuracy of the solution (Smerzini, 2010).

The Discontinuous Galerkin (DG) technique is implemented in SPEED as a non-conforming discretization approach to develop a flexible numerical strategy necessary to model large-scale, heterogeneous, and complex media. The DG is coupled with the SE formulation in SPEED to deal with non-uniform polynomial degree distributions and locally varying mesh sizes, employed at subdomain levels (conforming on each subdomain) (Mazzieri et al., 2013). Our model is composed of three parts: the geotechnical bedrock, the soil, and the buildings. The DG method will allow us to connect these different subdomains.

2.3.2 Material characterization of the soil

Because inelastic soil behavior in sandy soils starts at very low deformations, any moderate to severe earthquake will trigger material inelastic soil effects. The standard way to characterize the nonlinear dynamic behavior of the soils is through the shear modulus degrading and damping increasing curves as functions of the cyclic shear strain. To obtain these curves, laboratory tests were conducted on remolded soil samples from a borehole in the area. They were classified as SW-SM, according to USCS. The shear modulus and damping curves were obtained from combined resonant column (RC) and torsional shear (TS) tests performed at confinement pressures of 100 and 200 kPa. Because the water table is close to the surface in this area, these tests were performed under an undrained assumption. The obtained values are shown in Figure 2-3.

One of the main aspects affecting modulus degradation and damping increasing curves of granular soils is the mean effective confining stress (σ'_m) (Zhang, et al., 2005). For this reason, we adopted a modeling strategy, including a confining correction for this curve. In the selected area, the maximum basin depth is about 110 meters, corresponding to confining stress of about 900 kPa. Based on the laboratory results, a hyperbolic model was calibrated, following the normalized shear modulus:

$$\frac{G}{G_{max}} = \frac{1}{1+\left(\frac{\gamma}{\gamma_r}\right)^a} \text{ (2); } \gamma_r = \gamma_{r1}\left(\frac{\sigma'_m}{P_a}\right)^k \text{(2-3)}$$

This model was first proposed by Darendeli (2001). The value a is denoted the second curve-fitting variable, associated to the curvature. The γ_r is the reference strain when

$\frac{G}{G_{max}} = 0.5$, that can vary significantly with confinement. Therefore, the relation in Equation 2-3 is adopted to account for the in-situ confinement stress.

For convenience, the damping ratio was approximated as a quadratic function of the shear modulus degradation curve, with the form of Equation 2-4 and 2-5 (Zhang et al., 2005).

$$D\ (\%) = \mathrm{A}\left(\frac{G}{G_{máx}}\right)^2 + \mathrm{B}\ \left(\frac{G}{G_{máx}}\right) + \mathrm{C} + D_{mín}\ \text{(2-4)} \qquad D_{mín} = D_{min1}\left(\frac{\sigma'_m}{P_a}\right)^{-\frac{k}{2}} \text{(2-5)}$$

Table 2-1: Selected parameters for the hyperbolic model.

Parameter	$\boldsymbol{a}$	$\boldsymbol{k}$	**A**	**B**	**C**	$\boldsymbol{D_{min1}}$ (%)
Value	0.8	0.87	4.2	-16.9	13.5	1.5

The parameter summarized in Table 1 were calibrated based on our experimental results. The coefficients A, B and $C,$ were selected in the next order: the value of C minus D_{min1}=15%, predicts the maximum damping at high strains when G/G_{max} reach its residual value. Then, A and B define the best-fit curve for the measured values.

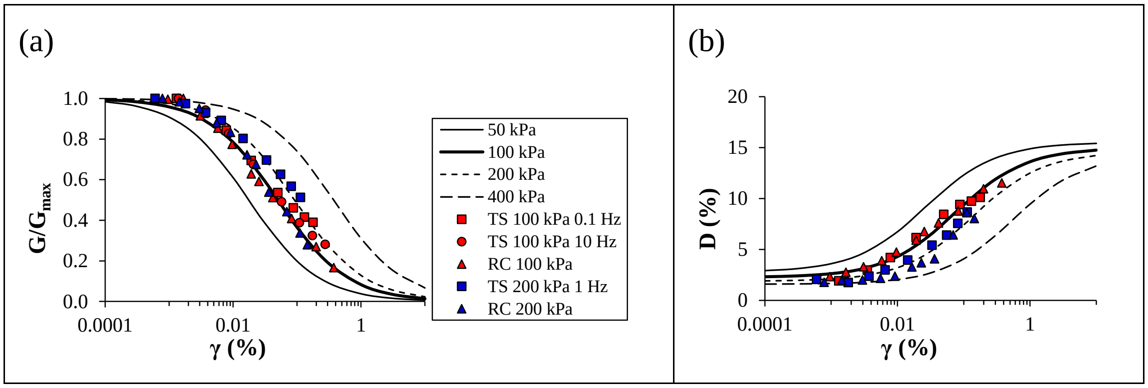

Figure 2-3: (a) Degradation and (b) damping curves for the material. A hyperbolic model was used to estimate the depth-varying curves, calibrated with laboratory tests for soil samples in the area.

The comparison of the proposed model against experimental data and confinement effect is shown in Figure 2-3. Additionally, the previous expression allows incorporating the impact of the overburden pressure induced by the buildings' weight. As the soil unit weight is known and with an estimation of the building weight based on its number of stories and underground levels, the vertical stress can be computed at any point in the soil domain.

2.3.3 Approximate nonlinear soil behavior modeling

The nonlinear behavior of the soil in our model was estimated by the Linear Equivalent Method, first proposed for a one-dimensional wave propagation problem (Schnabel et al, 1972). The method approximates the nonlinearity using an iterative procedure that calculates the dynamic properties (shear modulus and damping) according to the shear strains at various levels of the soil. The LEQ method procedure in SPEED was previously implemented by Muñoz et al. (2018). For each iteration, the average maximum shear strain at the center of the element is computed based on the principal strains. The factor $R_w = 0.65$ reduce the maximum shear strain to obtain the effective shear strain.

$\gamma_{max} = \max(|\varepsilon_1 - \varepsilon_2|, |\varepsilon_1 - \varepsilon_3|, |\varepsilon_2 - \varepsilon_3|)$; $\gamma_{eff} = R_w \times \gamma_{max}$ (2-6)

The modulus and damping, in terms of shear wave (Vs) and quality factor (Q), are updated, and the model is recomputed until a 5% difference was obtained at each monitor in the soil domain.

2.3.4 Building Properties

Each building is modeled as an elastic solid volume with a uniform density of $300 \frac{kg}{m^3}$ and a damping factor of 0.05, average values used in previous site-city investigations (Isbiliroglu, Taborda, & Bielak, 2015; Mazzieri et al., 2013). Each volume was discretized in several solid elements of vertical dimension equivalent to about 2 stories of the real building. This value reasonably agrees with the one ton per square meter usually adopted for seismic design in Chilean practice. The $v_p = 1.65\, v_S$ relationship was assumed to relate the compressional wave velocity to the shear wave velocity. These properties were used to obtain a shear wave velocity for each building through the calculation of the normal elastic modes. Full fixity at the bottom of each model was assumed to compute normal modes. The velocity was chosen, matching the first mode with the previously estimated natural frequency of each building. The values obtained vary from 200 to 650 m/s.

Table 2-2: Properties of the selected buildings.

Building ID	**Number of stories**	**Predicted T (s)**	**Modeled T_m (s)**	**G (MPa)**	**T0 (s)**
110	8	0.40	0.38	100	0.99
112	8	0.40	0.37	100	1.10
176	4	0.20	0.19	51	1.16
188	7	0.35	0.34	100	1.07
193	4	0.20	0.18	51	1.09
195	19	0.95	0.91	204	1.04
207	4	0.20	0.18	74	1.07
208	11	0.55	0.56	165	1.09
211	4	0.20	0.18	74	1.01
212	4	0.20	0.20	74	1.02
228	4	0.20	0.18	51	1.10
229	10	0.50	0.47	204	1.16
447	12	0.60	0.55	74	1.13
448	8	0.40	0.39	74	1.06
450	18	0.90	0.86	165	1.08
535	5	0.25	0.24	74	1.05
536	7	0.35	0.35	100	1.12
537	9	0.45	0.45	294	1.15
538	9	0.45	0.46	247	1.20
539	3	0.15	0.16	33	1.15
559	4	0.20	0.20	51	1.19

2.3.5 Mesh

Due to the limitation of computational resources, we selected a reduced area containing the most damaged buildings. The model includes 22 buildings located above an average sediment thickness of 90 to 105 meters in central Viña del Mar. The approximate spatial location of the model is shown in Figure 2-2a and the mesh in Figure 2-4a. The natural periods of the structures are in the range of 0.15 to 0.95 s. The predominant period of the soil in the same area is from 0.9 to 1.2 s, some site-building resonance effects are anticipated.

Table 2-3: Material parameters.

Material	V_s **(m/s)**	V_p **(m/s)**	Q_s	Q_p	ρ **(kg/m**^{3}**)**
Buildings	200 - 600	374 - 1122	10	20	300
Basin	function of the confinement (Eq. 2-3)				1800
Bedrock	900	1690	500	1000	2200

The non-conforming mesh was created entirely by the software Trelis®. The model has a total of 1,757,851 spectral nodes and 25,487 hexahedral elements, with a varying size from 1.7 to 5 meters. As the inelastic soil behavior tends to concentrate on the shallow layers, a more refined mesh was used for the upper 25 meters. Hence, the not-honoring approach is implemented in the soil, where the size of the mesh changes from 5x5 square meters in the top of the layer to 20x10 square meters in the deepest part of the model.

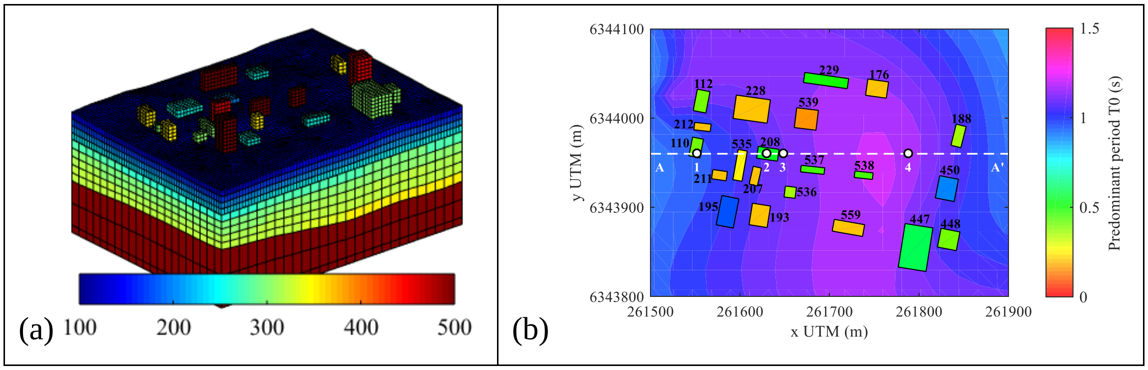

Figure 2-4: (a) mesh used to study the complex SCI effects in the area. The color bar represents the shear wave velocity used to model the soil and the buildings, calibrated with the number of stories rule and (b) Modeled structures period (Tm) and predominant soil period (T0) in the model.

The maximum target frequency for the model was 15 Hz. To obtain reliable results, the maximum size of the elements was checked, based on the criteria for the maximum characteristic dimension of the spectral element, for the spectral degree N=4, and G_λ=3 points of per minimum wavelength:

$\Delta l = \frac{\lambda}{G_\lambda} N$ (2-7)

Using this criterion, the maximum sizes vary from 13.3 to 63.3 meters for the buildings. At the bottom of the model, to introduce the seismic loading, a fictitious layer is used to introduce a perfectly vertical incident plane-wave front as a Neumann condition. Dirichlet boundary conditions were used only at the lateral boundaries to ensure shear-beam kinematics. An absorbing boundary condition was used to minimize wave reflections at the base of the model.

2.3.6 Input

The Viña Centro Seismic Station (VC), located above approximately 30 meters of sediments within the studied area, recorded the 1985 and 2010 earthquakes (Podestá et al., 2019). To reduce the running time, a modified Ricker wavelet was used as input motion, propagated in the N-S direction and calibrated to match with the response spectra associated with records available at this station. The analytic expression of this wavelet is the following (Li, Dong, & Zhao, 2014):

$R(t) = A \times \frac{1}{f_1 - f_0} [\, f_1 e^{-\pi^2 f_1^2 (t-t_0)^2} - f_0 e^{-\pi^2 f_0^2 (t-t_0)^2}]$(2-8)

This motion has a broader frequency band spectrum than the standard Ricker wavelet, and it has been widely used in wave propagation problems. Two input motions have been selected, R2 and R5, to cover different frequency bands. The first input (R2) was chosen to cover approximately the frequency range of available records at the VC station, while the second (R5) was used to cover the range of fundamental frequencies of the building located in the area. Table 4 shows the used parameters.

Table 2-4: selected parameters for modified Ricker wavelets.

Ricker	f_0 **(Hz)**	f_1 **(Hz)**	**Maximum frequency (Hz)**
R2	0.2	2.0	6.0
R5	0.5	5.0	16.0

To calibrate the amplitude of the input Ricker motions, we developed a simplified 1D column model at the exact location of the available records (VC station) using the inelastic soil model previously described. The amplitude was adjusted to have the same PGA than available records. The results of this procedure are shown in Figure 2-5.

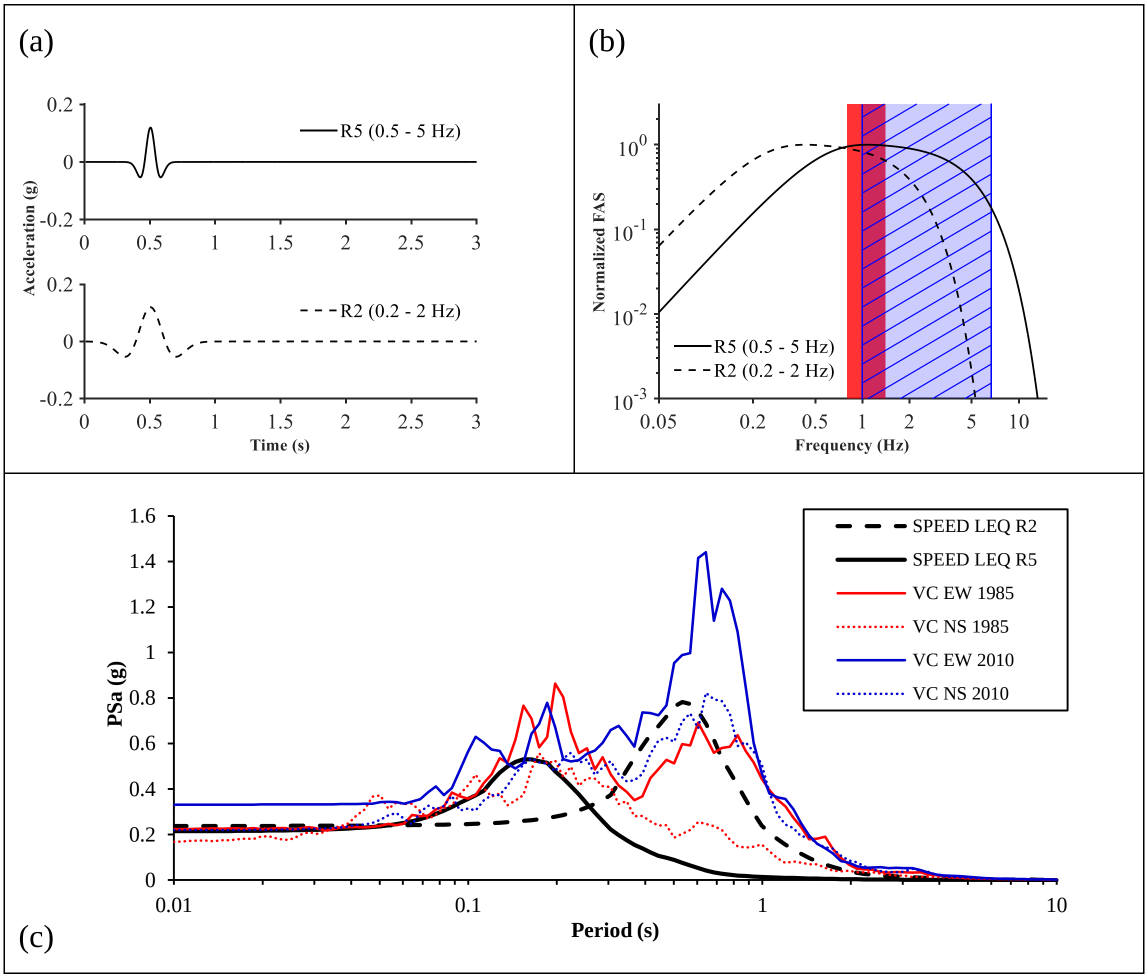

Figure 2-5: (a) Modified Ricker pulses used, both with two characteristic frequencies of 0.2 and 2 Hz and 0.5 y 5 Hz (R2 and R5). (b) Normalized Fourier amplitude spectrum of the input. The red area shows the range of predominant frequencies of the soil, and the fixed-base natural frequencies of the selected buildings are shown in the hatched blue area. (c) Pseudo Spectral Acceleration of available records and those associated with selected wavelets.

2.4 RESULTS

This work aims to understand the local effects produced by the multiple interactions between embedded buildings and the surrounding soil in a realistic urban setting, the city of Viña del Mar. Therefore, three different configurations were modeled. The first model has a fully coupled system between the buildings and the 3D model of the soil ($3D_{FC}$); and two settings that will work as uncoupled models: the 3D model of the soil without the buildings ($3D_U$), and multiple 1D columns ($1D_U$) with the same properties of the 3D model, where the evaluation of the building's response is analyzed separately after the extraction of the ground motion. The $3D_{FC}$ model includes both site-city (SCI) and soil-structure (SSI) interaction. The second model ($3D_U$) assesses the role of the basin spatial variation in the domain, while the third ($1D_U$) only includes the amplification due to the wave propagation in soil layers. Figure 6a illustrates the three different approaches. The local effects will be compared in terms of the modification of the ground motion and the structural response. For the structural response of the buildings of the uncoupled models, the time history was computed on SDTools®, a Structural Dynamic toolbox available for Matlab®, analyzing fixed-based models. The input was the motion that resulted from the wave propagation in the $3D_U$ and $1D_U$ models extracted from monitors located at the same depth as the foundation. In this case, two boundary conditions are applied to the bottom of the structural model:

- Case A: The nodes associated with the embedded degrees of freedom (DOFs) that are in contact with the soil are clamped (see Figure 2-6b Case A in red). This case assumes infinite stiffness from the adjacent soil.
- Case B: The nodes associated with the structure's bottom DOFs are clamped (see Figure 2-6b Case B in red). This case pretends to simulate full fixation only at the base.

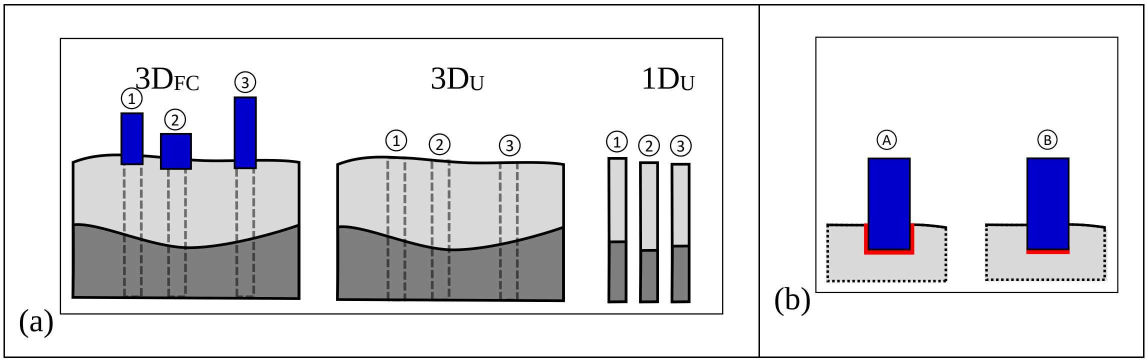

Figure 2-6: (a) Model approaches for the soil. From left to right: 3D fully coupled model (3DFC), 3D uncoupled model (3DU) and multiple 1D columns (1DU) and (b) Model approaches

Usually, Chilean reinforced concrete shear-wall buildings have perimetral basement walls of at least 60 cm of thickness to support the soil and the shallow water table pressures, i.e. lateral and bottom foundation could be considered as rigid (Case A). In the Chilean practice, soil interaction is usually neglected and the building model for modal analysis is assumed clamped at its base (Case B). Nevertheless, sometimes lateral interaction is included to seismically verify walls in contact with surrounding soil by adding elastic springs on lateral boundaries. This last situation is modeled in a more rigorously manner through $3D_{FC}$. Hence, combinations $3D_U$+A/B and $1D_U$+A/B try to be close to the standard modelling assumptions used in seismic building design.

2.4.1 Comparative analysis of the modification of the ground motion

To evaluate the effects of the buildings' inclusion on intensity parameters associated with the damage potential, a comparison between $3D_{FC}$ and $3D_U$ at the surface have been calculated in terms of three parameters: 1) the Peak Ground Acceleration (PGA) and the Peak Ground Velocity (PGV), to compare the amplitude of the ground motion; 2) the

Arias Intensity, an energy measure that considers the ground acceleration amplitude its duration and, 3) indirectly, the frequency content (Arias, 1970). The results for the three-dimensional model are shown in Figure 2-7 and Figure 2-8 for the inputs R2 and R5, respectively.

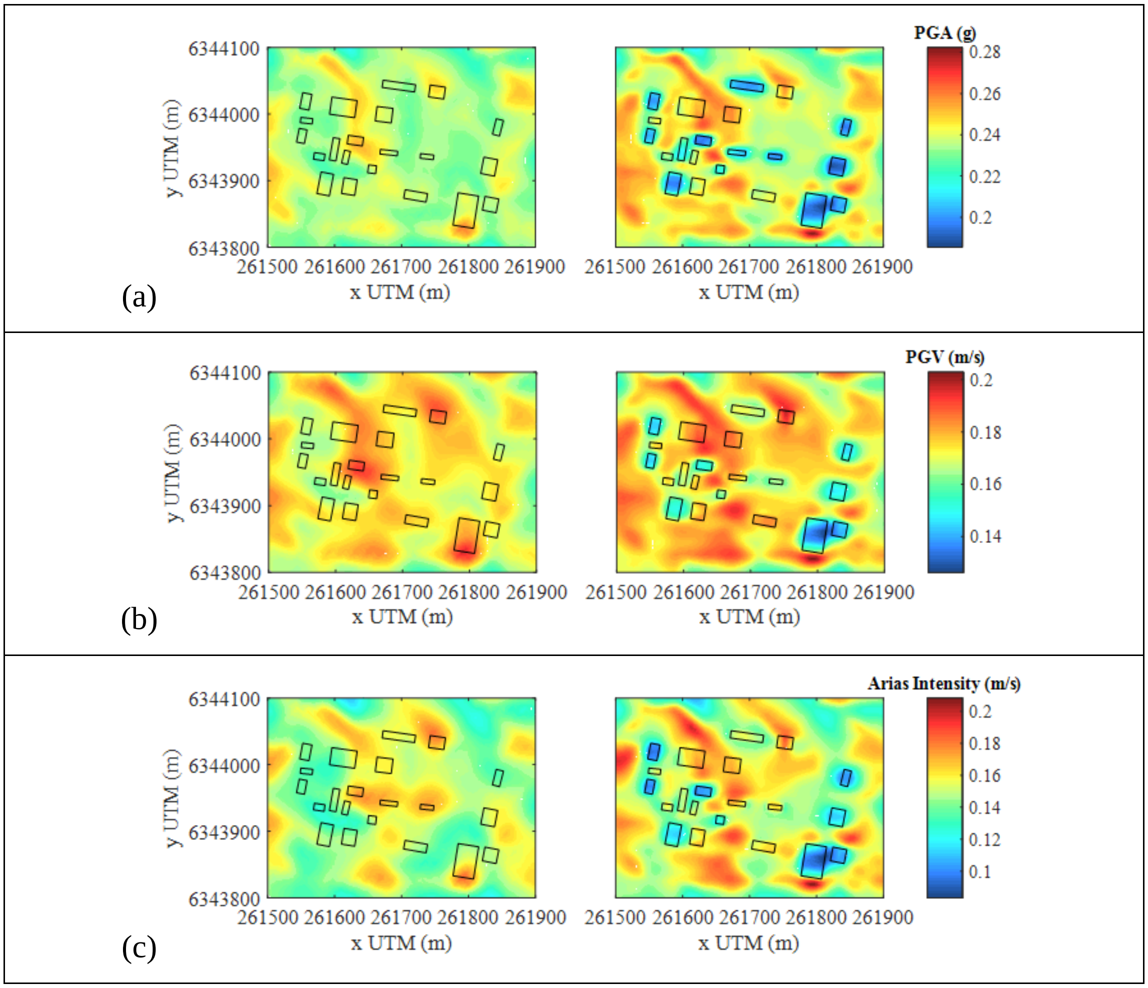

Figure 2-7: Seismic parameters to describe and compare ground motion, input R2: (a) PGA (g), (b) PGV (m/s) and Arias Intensity (m/s) for 3DU (left) and 3DFC (right) models. The buildings boundary in black, just for reference in the 3DU case.

In general, the spatial distribution for both cases is similar for all the calculated parameters. It can be noted that the tridimensional variation of the basin depth across the modeled domain is not sufficient to generate a significant difference in the free field motion, since the values show a moderate variation across the surface in the $3D_U$ models, from 0.21 to 0.26 g for the PGA, from 0.15 to 0.19 m/s for the PGV and from 0.11 to 0.18 m/s for the Arias Intensity. In the $3D_{FC}$ models, the inclusion of the site-city effects generates a general decrease at the building's base and in its surroundings. In this case, the PGA varies from 0.19 to 0.28 g, the PGV from 0.13 to 0.21 m/s, and the Arias Intensity from 0.08 to 0.21 m/s. However, this decrease is observable only in buildings with more than five stories, highlighting the importance of the building weight. This result agrees with the results from other investigations (Taborda, 2010).

Additionally, in the most densely populated sector, limited by UTM coordinates 261550 and 261650 in the East-West direction and 6343900 and 6344000 in the North-South direction, the frequency content of the propagated input is determinant. While in the R2 record the free-field motion decreases with the multiple interactions, the higher frequencies of the R5 record create enclosed areas where the energy is concentrated, especially where buildings are closest to each other.

Figure 2-9 shows the ratio for the same parameters, to quantify the difference in the buildings' incorporation. All the parameters show a decrease in the highest structures' local surroundings, represented by the blue colors. This deamplification in the R2 case is mainly oriented on the north-south (X) direction, the same direction of the propagated wave. PGA and PGV values outside the constructed area do not show significant change, while the energy of the motions at surface in the more densely area increases up to 23%. In the R5 case, the propagated energy increases up to 50% in the more densely area, and no deamplification is found.

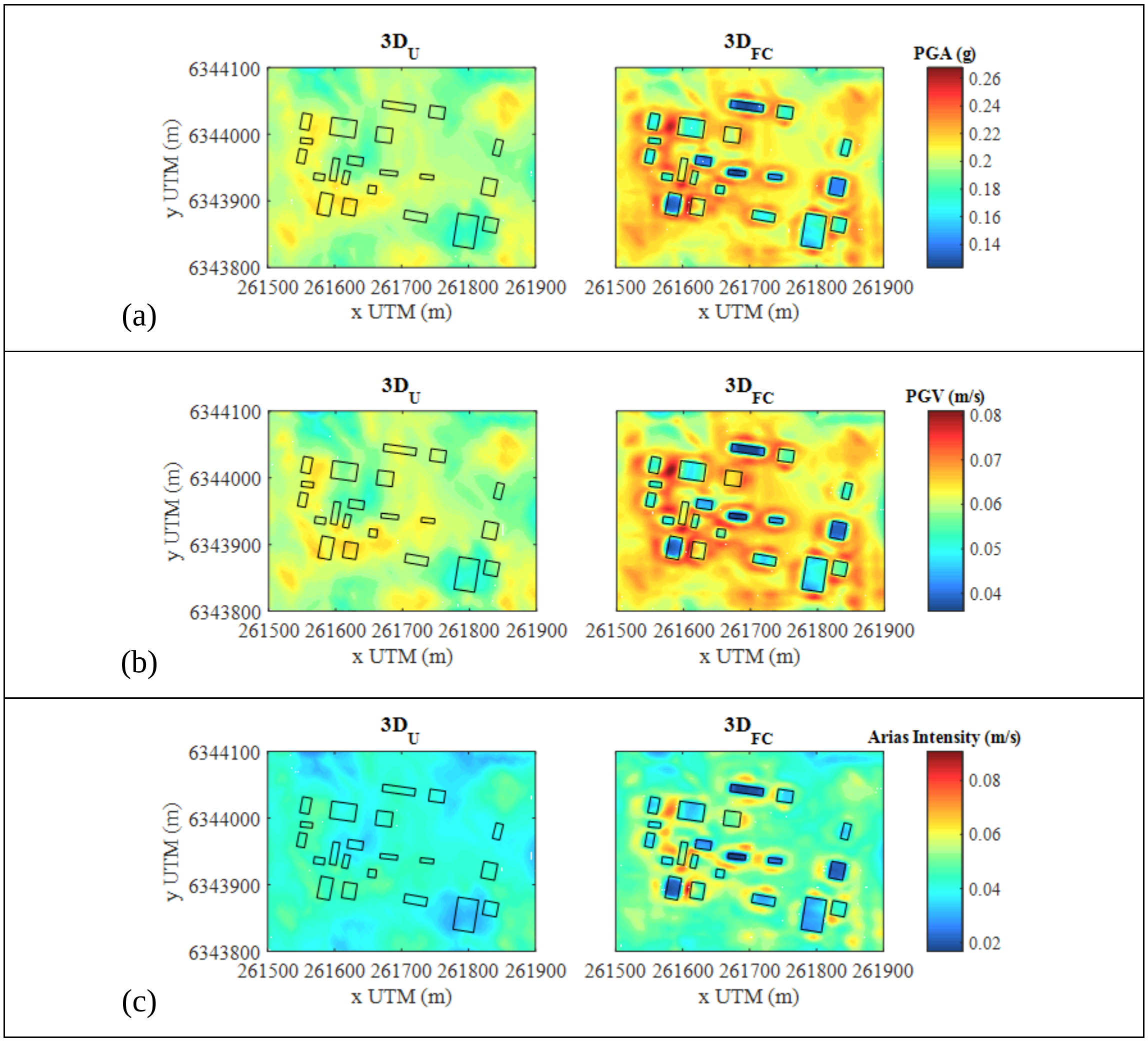

Figure 2-8: Seismic parameters to describe and compare ground motion, input R5: (a) PGA (g), (b) PGV (m/s) and Arias Intensity (m/s) for 3DU (left) and 3DFC (right) models. The buildings boundary in black, just for reference in the 3DU case.

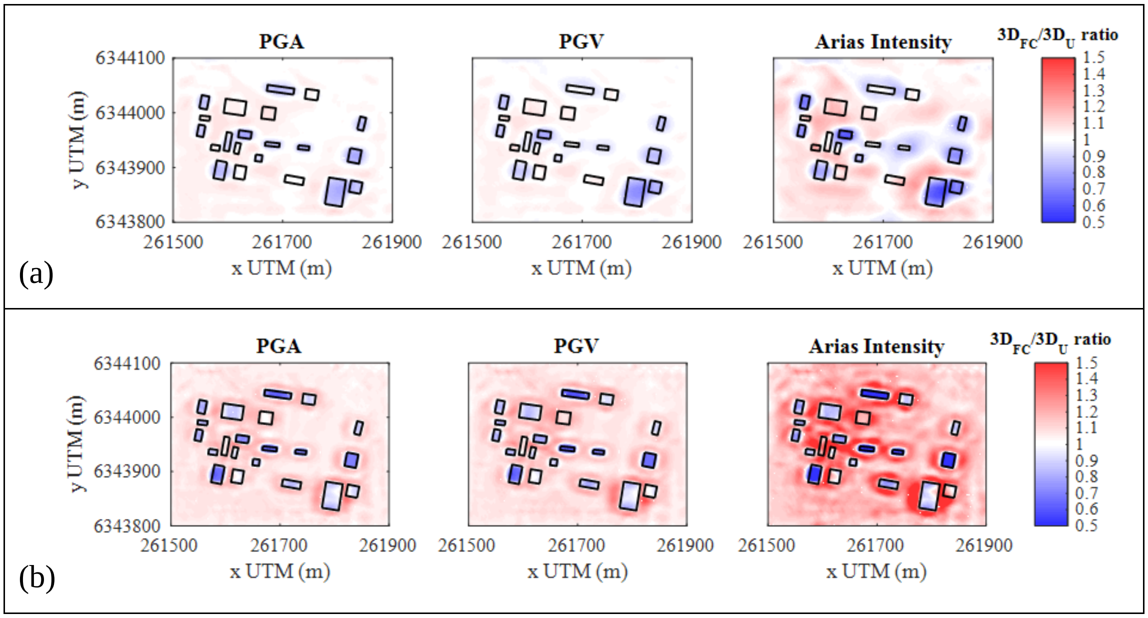

Figure 2-9: 3DFC/3DU Ratio for PGA, PGV and Arias Intensity at the surface. Inputs (a) R2 and (b) R5.

The degree of nonlinearity in the soil can be examined through the maximum strain at different depths, reached for the R2 and R5 records in the last iteration of the LEQ procedure. Figure 2-10a and Figure 2-10b show a cross-section across the A-A' profile in the middle of the model, for the R2 and R5 propagation, respectively. The spatial variability of the shear strain is localized near buildings, while no significant lateral variability is observed far enough from buildings, i.e. where free field condition is approximately satisfied. For the input R2, the maximum shear strains are situated at depths of 10-20 meters. Due to an increase of confinement, the maximum strain decreases below the structures but increases in the surrounding elements at the free surface. The impact of the buildings on the level of non-linearity is not appreciable below 35 meters. Nevertheless, for the input R5, the maximum strains are located on the surface, but maximum values are half of the value of those obtained for R2 input. This observation illustrates the influence of the frequency content of the input on energy dissipation in the soil. From Figure 2-10b, it is clear that the major influence of the buildings' motions is concentrated in the upper layers of the model. Because of low confinement, this portion of soil has a limited stiffness i.e. it is more prone to be influenced by lateral motion of the embedded portion of buildings.

The maximum strain has been extracted from profiles x_1 and x_2, located below buildings ID110 and ID208, as well as x_3, located immediately next to building ID208 and x_4, located sufficiently far from the influence of any structure (see Figure 2-4b). Figure 2-10b and Figure 2-10d show the degradation curves at different confinements. The higher levels of degradation (about 40%) are found in a combination of high strains and low confinements, in the shallow layers of the model.

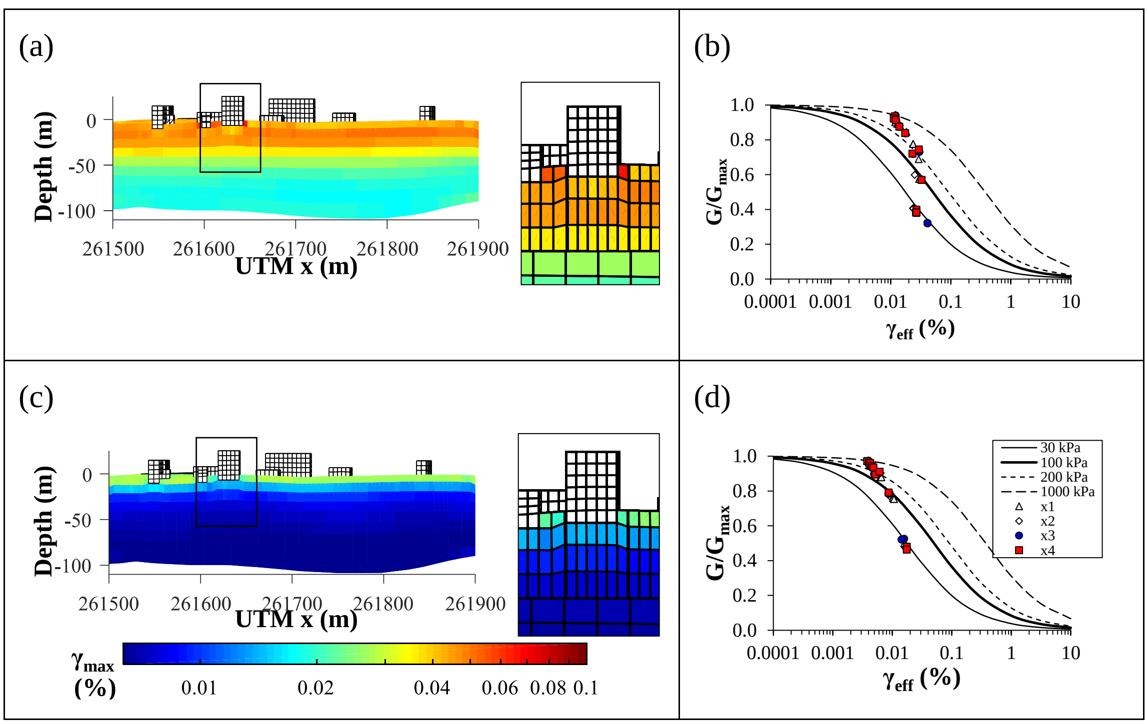

Figure 2-10: (a and c) Distribution of shear strain in 3DFC model and selected profiles x1 to x4 (b and d) Shear modulus degradation at different depths, extracted from profiles, for R2 and R5, respectively.

2.4.2 Structural response on selected buildings

In a single building, the presence of the surrounding soil affects the motion of the structures due to the inertial and kinematic effects (NEHRP, 2012). Partial embedment could increase these effects because of lateral interaction between the building and the lateral soil. In addition to this effect, multiple interactions between buildings are modeled in the $3D_{FC}$ case.

To compute the building's response, in the $3D_{FC}$ case, the base motion was subtracted to absolute displacement of structural nodes to obtain the relative motion to surrounding soil. For the uncoupled approaches, a separated finite element model was solved in a time domain for each building to compute seismic lateral displacements. This separated model has the same geometry and material properties as those used in $3D_{FC}$ model. Because of partial embedment, the acceleration obtained at 5 meters depth from the surface has been extracted from $3D_U$ and $1D_U$ cases. The damping matrix was calculated as 5% of Rayleigh damping. The boundary conditions for these models, shown in Figure 2-6, were selected to represent different lateral interaction between the soil and structure.

Four cases of buildings were selected to illustrate tendencies (ID195, ID207, ID208, and ID450). The time response of the relative roof displacement and the interstory drift were calculated. Figure 2-11 display the results for R2 case of the selected building, while Table 2-5 summarizes the maximum values of all the modeled buildings for the same input R2; the results for R5 are shown in Table 2-6. These results share the same behavior as R2, but they reach smaller magnitudes due to the high frequency of the input.

Table 2-5: Comparison of the maximum responses for the structures in the area, input R2.

ID	Maximum roof displacement (cm)					Maximum Interstory Drift (x10^{-3})				
	$1D_U$ Case A	$1D_U$ Case B	$3D_U$ Case A	$3D_U$ Case B	$3D_{FC}$	$1D_U$ Case A	$1D_U$ Case B	$3D_U$ Case A	$3D_U$ Case B	$3D_{FC}$
110	3.08	4.28	3.08	4.17	3.89	1.82	2.15	1.82	2.08	2.12
112	2.19	4.13	2.25	3.99	3.51	1.33	2.03	1.37	1.96	1.94
176	0.24	1.06	0.25	1.15	0.72	0.20	0.79	0.21	0.85	1.42
188	1.28	3.73	1.29	3.68	3.15	0.92	2.09	0.92	2.06	1.97
193	0.26	1.24	0.27	1.33	0.79	0.23	0.94	0.23	1.01	0.64
195	4.72	4.98	4.67	4.65	3.80	1.42	1.33	1.43	1.34	1.18
207	0.16	2.22	0.16	2.24	0.81	0.17	1.75	0.17	1.76	0.61
208	2.33	3.65	2.40	3.98	3.74	1.01	1.37	1.04	1.49	1.44
211	0.22	0.83	0.22	0.86	0.75	0.18	0.63	0.19	0.65	0.80
212	0.18	0.73	0.19	0.76	0.65	0.17	0.55	0.17	0.57	0.51
228	0.31	0.70	0.31	0.72	0.69	0.32	0.66	0.32	0.68	0.68
229	0.65	1.00	0.62	0.97	1.09	0.30	0.40	0.29	0.39	0.42
447	4.17	4.23	4.64	4.75	3.77	1.56	1.54	1.74	1.61	1.44
448	2.24	3.96	2.18	3.94	3.13	1.27	1.86	1.23	1.85	1.60
450	4.75	4.70	4.79	4.73	3.96	1.46	1.41	1.47	1.42	1.21
535	0.44	2.83	0.45	2.94	1.70	0.45	2.03	0.47	2.12	1.42
536	1.72	4.01	1.79	4.17	3.78	1.17	2.26	1.22	2.35	2.32
537	0.38	0.91	0.39	0.92	1.22	0.19	0.37	0.19	0.38	0.60
538	0.67	1.86	0.69	1.94	2.21	0.34	0.79	0.35	0.83	0.96
539	0.20	0.79	0.20	0.78	0.59	0.23	0.82	0.23	0.82	0.91
559	0.29	0.77	0.29	0.80	0.68	0.24	0.69	0.24	0.70	0.65

Table 2-6: Comparison of the maximum responses for the structures in the area, input R5.

ID	Maximum roof displacement (cm)					Maximum Interstory Drift ($x10^{-3}$)				
	$1D_U$ Case A	$1D_U$ Case B	$3D_U$ Case A	$3D_U$ Case B	$3D_{FC}$	$1D_U$ Case A	$1D_U$ Case B	$3D_U$ Case A	$3D_U$ Case B	$3D_{FC}$
110	0.59	0.59	0.62	0.61	0.54	0.38	0.38	0.42	0.42	0.48
112	0.56	0.60	0.61	0.64	0.53	0.36	0.36	0.41	0.41	0.44
176	0.26	0.52	0.22	0.53	0.39	0.23	0.39	0.19	0.40	1.66
188	0.55	0.56	0.55	0.57	0.52	0.39	0.35	0.40	0.37	0.45
193	0.31	0.56	0.35	0.59	0.43	0.28	0.43	0.32	0.46	0.37
195	0.54	0.50	0.59	0.53	0.42	0.28	0.26	0.32	0.29	0.24
207	0.15	0.58	0.14	0.57	0.47	0.17	0.48	0.16	0.47	0.50
208	0.58	0.61	0.52	0.56	0.49	0.29	0.29	0.24	0.25	0.27
211	0.21	0.51	0.29	0.54	0.43	0.18	0.39	0.25	0.41	0.38
212	0.17	0.48	0.25	0.55	0.43	0.16	0.37	0.23	0.42	0.37
228	0.29	0.45	0.30	0.45	0.40	0.28	0.39	0.29	0.39	0.36
229	0.45	0.49	0.43	0.46	0.34	0.21	0.19	0.20	0.18	0.15
447	0.55	0.52	0.54	0.52	0.38	0.32	0.30	0.30	0.29	0.26
448	0.56	0.60	0.53	0.57	0.50	0.37	0.37	0.33	0.34	0.42
450	0.56	0.52	0.56	0.52	0.38	0.31	0.29	0.30	0.28	0.24
535	0.37	0.56	0.39	0.58	0.51	0.40	0.43	0.41	0.44	0.56
536	0.60	0.61	0.63	0.65	0.56	0.42	0.39	0.43	0.43	0.48
537	0.36	0.51	0.36	0.51	0.40	0.18	0.21	0.18	0.22	0.19
538	0.47	0.53	0.52	0.56	0.47	0.24	0.23	0.27	0.25	0.25
539	0.21	0.51	0.18	0.49	0.42	0.22	0.50	0.20	0.49	0.46
559	0.27	0.45	0.27	0.45	0.36	0.24	0.37	0.23	0.37	0.32

From previous results, it can be noted that they are no significant differences between the $1D_U$ and $3D_U$ cases because on the modeled area the basin has an approximate uniform thickness, i.e. the soil is almost 1D. Nevertheless, some more pronounced differences could be noted between $3D_{FC}$ and Case A or Case B.

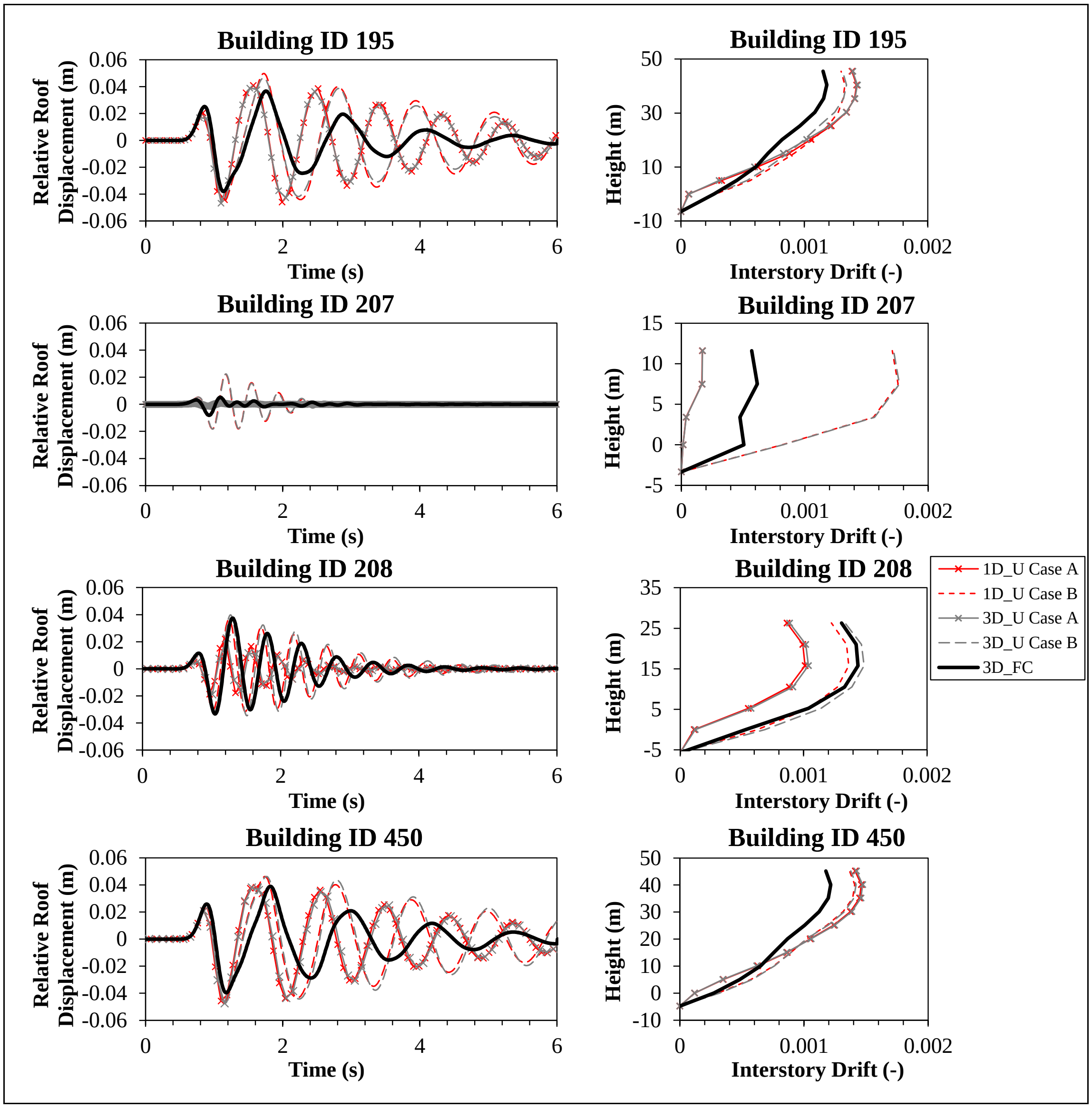

Figure 2-11: Relative roof displacement (left) and internode drift (right) of selected buildings, ID195, 207, 208 and 450, for the input R2.

In general, the type of differences depends on the number of stories:

- Lower buildings (3 to 4 floors as ID207) have the greatest variation when considering the two different levels of embedment. The response of Case A decreases up to 20% compared to Case B, maybe because it reacts as a rigid body when most of its DOFs are fixed. In these buildings, the $3D_{FC}$ response is in between both fixed base hypotheses, so the ground surrounding the building partially restricts the motion.

- The behavior of medium-high buildings (like ID208) in $3D_{FC}$ is much closer to Case B, horizontally fixed at the base. Hence, considering lateral fixity would generate non-conservative responses, reducing by 30 to 70% both the maximum drift and the roof displacement, as seen in Figure 2-11.
- Higher buildings, like ID 195 and 450, are almost in resonance with the soil according to Figure 2-4b. Nevertheless, the inclusion of the SCI effects is beneficial, since cases A and B achieve higher values of roof displacement. In terms of group effects, ID 195 is located within the densest area while ID 450 is more isolated and the same tendency is found. Consequently, group effects seem to be negligible.

Three buildings of the studied set increase their seismic demands (ID 229, 537, and 538), when the SCI effects are considered. All, as shown in Figure 2-4b, have a high floor plan aspect ratio, defined as the longitudinal dimension divided by its transverse dimension of the floor plan (Jünemann et al., 2015), and they are oriented, in terms of their principal direction, opposite to the direction of loading.

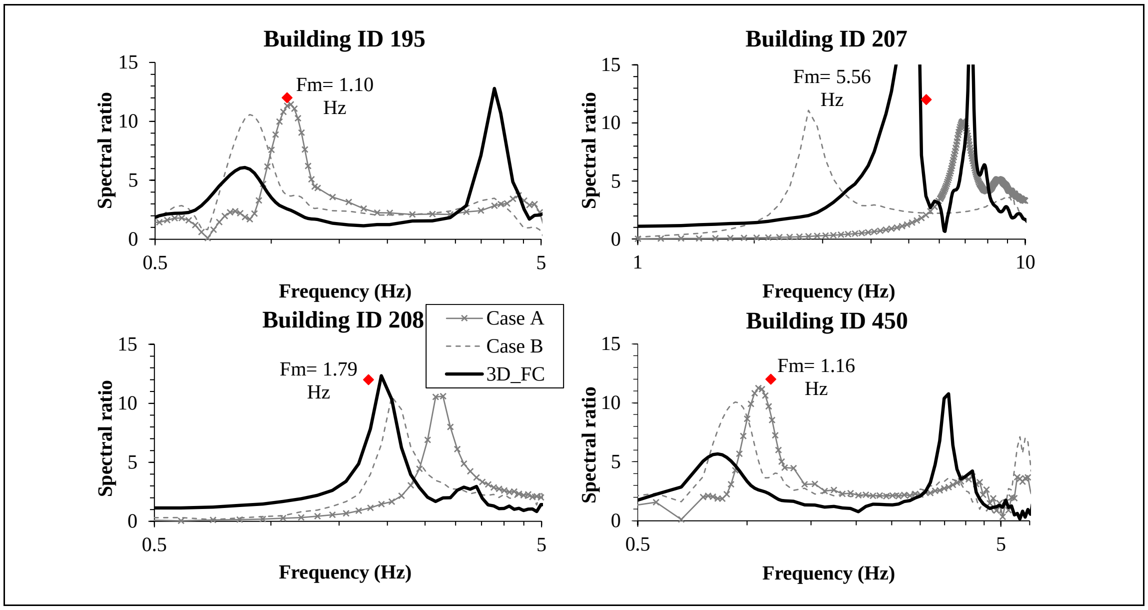

Figure 2-12: Spectral ratio of the selected buildings' vibration for the 3 cases modeled. The red dot represents the building modeled resonant frequency F_m.

Figure 2-12 displays the spectral ratios between the top displacement and the base of each building considered. Additionally, we include the first mode resonant frequency (Fm) of each building assuming clamping at surface level, i.e. neglecting undergrounds.

The first spectral ratio peak shifts to lower frequencies compared to F_m for all buildings, except for the ID208 where the effect is negligible. Higher buildings (ID195 and 450) behave more flexible in the $3D_{FC}$ model because of soil flexibility, where the SCI effects are beneficial to the response. In these buildings, $3D_{FC}$ results also suggest the activation of a higher mode which is not observable in the other approaches.

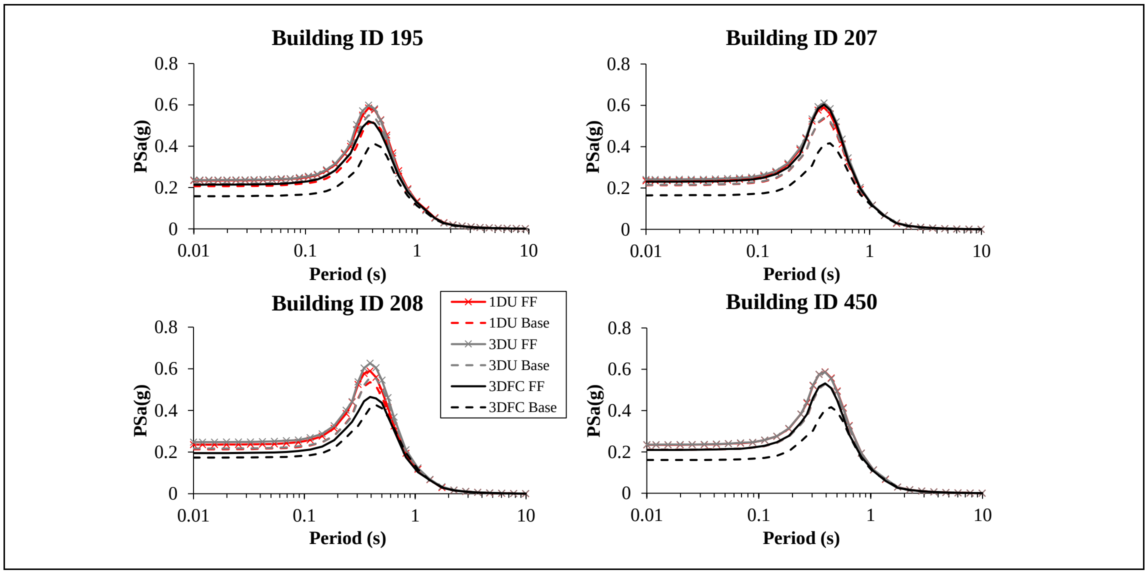

Figure 2-13: Pseudo Spectral Acceleration from monitors at the surface (FF) and foundation level (Base) for the three different approaches. The obtention of the accelerations in the $3D_{FC}$ is immediate, while for the uncoupled models ($1D_U$ and $3D_U$), the base level refers to a monitor located at the same depth as in $3D_{FC}$ model.

Figure 2-13 compares the 5% damped elastic response spectra (PSa) at the foundation level from the free-field, far enough from the structures in the $3D_{FC}$ model. First, no significant difference is obtained from 3D to 1D approaches, confirming the little depth variability that exists in the basin in the area analyzed. One of the reasons that the incorporation of the SCI effects is beneficial is the deamplification may exist at the base of the buildings; this may act as an input for the response history analysis. The reduction in PGA in uncoupled cases is approximately 10-12%, while in the $3D_{FC}$ case the decrease reaches up to 28%. The peak in the base is also shifted. The uncoupled cases only incorporate the embedment effects when the building is funded at a certain depth below the surface. This is when the response decreases with respect to the free-field.

2.5 CONCLUSIONS

A 3D seismic wave propagation model of the area of Viña del Mar city, where numerous buildings were damaged during the last Mw 8.8 earthquake, was developed to study SCI. This model includes buildings to evaluate the local interaction between multiple structures and the influence of SCI effects in a realistic urban environment.

For the creation of the model, the three-dimensional basin of the entire city of Viña del Mar was validated in a study by Podestá et al., (2019) using available records. Buildings were added, with properties also estimated by geophysics, the behavior of those buildings was confirmed by two previous investigations of the same city. We based our comparison on maximum roof displacement and maximum interstory drift, parameters that could be associated with structural damage, which at the same time agrees with the parameters used for the few studies on the subject.

The SCI effects are, in general, beneficial for most buildings. However, a few will suffer more damage as reported by Lu et al. (2018) and Taborda (2010). From the findings of the study, the following is clear: in larger buildings the response would be indifferent to the level of embedding of the base and, in these cases, the inclusion of site-city effects is beneficial. On the other hand, in buildings of less than 12 stories the total embedment of the base generates a significant decrease of the response. Thus, it is important to take into account the underground levels.

While the evaluation of SCI effects on buildings is complex, it is believed that the increase in confinement stresses resulting from the difference between the excavated soil and the weight of the building would be key to the decrease in response. With the increase in confinement, the properties of the soil under the foundation are stiffer, thus reducing deformation. This also highlights the need to consider the nonlinearity of the soil.

On the other hand, regarding soil to site resonance, the foundation flexibility modeled by the coupled approach introduces a frequency shift from resonance for buildings ID195 and ID450, avoiding this kind of amplification. From the results presented, underground levels have a significant influence on building response; future research will focus on a more detailed quantification of this specific aspect of the SCI problem.

Group effects, on the other hand, have to do with the interaction between buildings. Although the buildings themselves generate an obvious interference in their surroundings, their influence on other buildings was not clear. Future work will expand the domain to more dense and large areas to introduce basis boundaries and therefore include surface wave generation and their effects on SCI.

ACKNOWLEDGMENTS

This study is based upon work supported partially by the FONDEF project D10E1027 and partially by CIGIDEN (National Research Center of Integrated Natural Disaster Management) FONDAP 15110017.

REFERENCES

Aki, K. (1957). Space and time spectra of stationary stochastic waves, with special reference to microtremors. *Bulletin of the Earthquake Research Institute*. https://doi.org/http://hdl.handle.net/2261/11892

Amini, F., & Shadlou, M. (2011). Embedment effects of flexible foundations on control of structures. *Soil Dynamics and Earthquake Engineering*, *31*(8), 1081–1093. https://doi.org/10.1016/j.soildyn.2010.12.007

Antonietti, P. F., Mazzieri, I., Quarteroni, A., & Rapetti, F. (2012). Non-conforming high order approximations of the elastodynamics equation. *Computer Methods in Applied Mechanics and Engineering*, *209–212*, 212–238. https://doi.org/10.1016/j.cma.2011.11.004

Aranda, C., Vidal, F., Alguacil, G., Navarro, M., & Valverde-Palacios, I. (2014). Fundamental period and earthquake damage in RC buildings of Viña del Mar (Chile). *Proceedings of the International Conference on Structural Dynamic , EURODYN*, *2014-Janua*(July), 2955–2962.

Arias, A. (1970). A measure of earthquake intensity. In *Seismic Design for Nuclear Power Plants*.

Avilés, J., & Pérez-Rocha, L. E. (1998). Effects of foundation embedment during building-soil interaction. *Earthquake Engineering and Structural Dynamics*, *27*(12), 1523–1540. https://doi.org/10.1002/(SICI)1096-9845(199812)27:12<1523::AID-EQE798>3.0.CO;2-5

Carrasco, 0., & Nuñez, C. (2013). Microzonificación Sísmica de la ciudad de Viña del Mar. *Memoria Para Optar Al Título de Ingeniero Civil, Universidad Técnica Federico Santa María.*

Chávez-García, F. J., & Cárdenas-Soto, M. (2002). The contribution of the built environment to the “free-field” ground motion in Mexico City. *Soil Dynamics and*

Earthquake Engineering, *22*(9–12), 773–780. https://doi.org/10.1016/S0267-7261(02)00098-2

Darendeli, B. M. (2001). *Development of New Family of Normalized Modulus Reduction and Material Damping Curves*.

Garofalo, F., Foti, S., Hollender, F., Bard, P. Y., Cornou, C., Cox, B. R., … Vergniault, C. (2016). InterPACIFIC project: Comparison of invasive and non-invasive methods for seismic site characterization. Part II: Inter-comparison between surface-wave and borehole methods. *Soil Dynamics and Earthquake Engineering*, *82*, 241–254. https://doi.org/10.1016/j.soildyn.2015.12.009

Grimme, K., & Álvarez, L. (1964). *El suelo de fundación de Valparaíso y Viña del Mar. Boletín N°16.* Santiago Chile.

Hayashi, K. (2008). *Development of the Surface-wave Methods and Its Application to Site Investigations*. *Report*. Kyoto University. Retrieved from http://repository.kulib.kyoto-u.ac.jp/dspace/handle/2433/57255

INE, I. N. de E. (2017). Síntesis de resultados Censo 2017. INE Chile.

Isbiliroglu, Y., Taborda, R., & Bielak, J. (2015). Coupled soil-structure interaction effects of building clusters during earthquakes. *Earthquake Spectra*, *31*(1), 463–500. https://doi.org/10.1193/102412EQS315M

Jünemann, R., de la Llera, J. C., Hube, M. A., Cifuentes, L. A., & Kausel, E. (2015). A statistical analysis of reinforced concrete wall buildings damaged during the 2010, Chile earthquake. *Engineering Structures*, *82*, 168–185. https://doi.org/10.1016/j.engstruct.2014.10.014

Kham, M., Semblat, J. F., Bard, P. Y., & Dangla, P. (2006). Seismic site-city interaction: Main governing phenomena through simplified numerical models. *Bulletin of the Seismological Society of America*, *96*(5), 1934–1951. https://doi.org/10.1785/0120050143

Kumar, N., & Narayan, J. P. (2019). Quantification of Fundamental Frequencies of 3D

Basins and Structures and Site–City Interaction Effects on Responses of Structures. *Pure and Applied Geophysics*. https://doi.org/10.1007/s00024-019-02158-8

Kvaerna, T., & Ringdahl, F. (1986). *Stability of various f-k estimation techniques*. *Semmiannual technical summary*. Kjeller, Norway.

Leyton, Felipe, Ramírez, S., & Vásquez, A. (2012). USO Y LIMITACIONES DE LA TÉCNICA DE MICROVIBRACIONES (RHV) EN LA CLASIFICACIÓN SÍSMICA DE SUELOS. *VII Congreso Chileno de Geotecnia*.

Leyton, F., Ruiz, S., Sepúlveda, S. A., Contreras, J. P., Rebolledo, S., & Astroza, M. (2013). Microtremors' HVSR and its correlation with surface geology and damage observed after the 2010 Maule earthquake (Mw 8.8) at Talca and Curicó, Central Chile. *Engineering Geology*, *161*, 26–33. https://doi.org/10.1016/j.enggeo.2013.04.009

Li, X., Dong, L., & Zhao, Q. (2014). Seismic modelling study of P-wave attenuation and velocity dispersion in patchy-saturated porous media. *Journal of Geophysics and Engineering*, *11*(6). https://doi.org/10.1088/1742-2132/11/6/065010

Lu, X., Tian, Y., Wang, G., & Huang, D. (2018). A numerical coupling scheme for nonlinear time history analysis of buildings on a regional scale considering site-city interaction effects. *Earthquake Engineering and Structural Dynamics*, *47*(13), 2708–2725. https://doi.org/10.1002/eqe.3108

Mazzieri, I., Stupazzini, M., Guidotti, R., & Smerzini, C. (2013). SPEED: SPectral elements in elastodynamics with discontinuous galerkin: A non-conforming approach for 3d multi-scale problems. *International Journal for Numerical Methods in Engineering*, *95*(12), 991–1010. https://doi.org/10.1002/nme.4532

Midorikawa, S. (1990). *Ambient vibration tests of buildings in Santiago and Viña del Mar*. Santiago Chile: Departamento de Ingeniería Estructural Pontificia Universidad Católica de Chile.

Ministerio de Vivienda y Urbanismo. Decreto 61, Biblioteca del Congreso Nacional de

Chile § (2011). Chile. Retrieved from https://www.leychile.cl/N?i=1034100&f=2011-12-13&p=

Nakamura, Y. (1989). A Method for Dynamic Characteristics Estimation of Subsurface using Microtremor on the Ground Surface. *Quarterly Report the Railway Technical Research Institute*, (1), 25–33.

NEHRP Consultants Joint Venture. (2012). *Soil-Structure Interaction for Building Structures*. *Nist Gcr* (Vol. 12).

Panzera, F., Lombardo, G., & Muzzetta, I. (2013). Evaluation of building dynamic properties through in situ experimental techniques and 1D modeling: The example of Catania, Italy. *Physics and Chemistry of the Earth*, *63*, 136–146. https://doi.org/10.1016/j.pce.2013.04.008

Podestá, L., Sáez, E., Yáñez, G., & Leyton, F. (2019). Geophysical Study and 3-D Modeling of Site Effects in Viña del Mar, Chile. *Earthquake Spectra*, *35*(3), 1329–1349. https://doi.org/10.1193/080717eqs155m

Riddell, R., Wood, S. L., & de la Llera, J. C. (1987). *1985 CHILE EARTHQUAKE: STRUCTURAL CHARACTERISTICS AND DAMAGE STATISTICS FOR THE BUILDING INVENTORY IN VINA DEL MAR. Civil Engineering Studies, Structural Research Series (University of Illinois at Urbana-Champaign,.*

Ruiz, S., & Madariaga, R. (2018). Historical and recent large megathrust earthquakes in Chile. *Tectonophysics*, *733*(January), 37–56. https://doi.org/10.1016/j.tecto.2018.01.015

Sahar, D., Narayan, J. P., & Kumar, N. (2015). Study of role of basin shape in the site–city interaction effects on the ground motion characteristics. *Natural Hazards*, *75*(2), 1167–1186. https://doi.org/10.1007/s11069-014-1366-2

Schnabel, P. B., Lysmer, J., & Bolton Seed, H. (1972). *A COMPUTER PROGRAM FOR EARTHQUAKE RESPONSE ANALYSIS OF HORIZONTALLY LAYERED SITES*.

Smerzini, C. (2010). The Earthquake Source in Numerical Modeling of Seismic Wave

Propagation in Heterogeneous Earth Media.

Smerzini, C., Paolucci, R., & Stupazzini, M. (2011). Comparison of 3D, 2D and 1D numerical approaches to predict long period earthquake ground motion in the Gubbio plain, Central Italy. *Bulletin of Earthquake Engineering*, *9*(6), 2007–2029. https://doi.org/10.1007/s10518-011-9289-8

Taborda, R. (2010). *Three Dimensional Nonlinear Soil and Site-City Effects in Urban Regions*. Carnegie Mellon University.

Toledo, G. (2017). Aportes para una nueva zonificación geotécnica de Viña del Mar: Estimación de la amplificación sísmica en la cuenca del Marga-Marga. *Memoria Para Optar Al Título de Ingeniero Civil, Universidad Técnica Federico Santa María.*

Wathelet, M. (2008). An improved neighborhood algorithm: parameter conditions and dynamic scaling. *GEOPHYSICAL RESEARCH LETTERS*, *35*, 9301. https://doi.org/10.1029/2008GL033256

Wirgin, A., & Bard, P. Y. (1996). Effects of buildings on the duration and amplitude of ground motion in Mexico City. *Bulletin of the Seismological Society of America*, *86*(3), 914–920.

Zhang, J., Andrus, R. D., & Juang, C. H. (2005). Normalized shear modulus and material damping ratio relationships. *Journal of Geotechnical and Geoenvironmental Engineering*, *131*(4), 453–464. https://doi.org/10.1061/(ASCE)1090-0241(2005)131:4(453)